

Article

Physical and Mechanical Properties and Damage Mechanism of Sandstone at High Temperatures

Yadong Zheng ¹, Lianying Zhang ^{2,*}, Peng Wu ², Xiaoqian Guo ¹, Ming Li ³ and Fuqiang Zhu ³¹ School of Mechanics and Civil Engineering, China University of Mining and Technology, Xuzhou 221116, China² School of Physics and New Energy, Xuzhou University of Technology, Xuzhou 221018, China³ State Key Laboratory for Geomechanics and Deep Underground Engineering, China University of Mining and Technology, Xuzhou 221116, China

* Correspondence: zly@xzit.edu.cn

Abstract: The physical and mechanical properties of rocks change significantly after being subjected to high temperatures, which poses safety hazards to underground projects such as coal underground gasification. In order to investigate the effect of temperature on the macroscopic and microscopic properties of rocks, this paper has taken sandstone as the research object and conducted uniaxial compression tests on sandstone specimens at different temperatures (20–1000 °C) and different heating rates (5–30 °C/min). At the same time, the acoustic emission (AE) test system was used to observe the acoustic emission characteristics of the rock damage process, and the microstructural changes after high temperature were analyzed with the help of a scanning electron microscope (SEM). The test results show that the effect of temperature on sandstone is mainly divided into three stages: Stage I (20–500 °C) is the strengthening zone, the evaporation of water and the contraction of primary fissures, and sandstone densification is enhanced. In particular, the compressive strength and elastic modulus increase, the macroscopic damage mode is dominated by shear damage, and the fracture micromorphology is mainly brittle fracture. Stage II (500–600 °C) is the transition zone, 500 °C is the threshold temperature for the compressive strength and modulus of elasticity, and the damage mode changes from shear to cleavage damage, and the sandstone undergoes brittle–ductile transition in this temperature interval. Stage III is the physicochemical deterioration stage. The changes in the physical and chemical properties make the sandstone compressive strength and modulus of elasticity continue to decline, the macroscopic damage mode is mainly dominated by cleavage damage, and the fracture microscopic morphology is of a more toughness fracture. The effect of different heating rates on the mechanical properties of sandstone was further studied, and it was found that the mechanical properties of the rock further deteriorated under higher heating rates.

Keywords: sandstone; high temperature; heating rate; physical and mechanical properties; acoustic emission; macroscopic destructive characteristic; microscopic morphology



Citation: Zheng, Y.; Zhang, L.; Wu, P.; Guo, X.; Li, M.; Zhu, F. Physical and Mechanical Properties and Damage Mechanism of Sandstone at High Temperatures. *Appl. Sci.* **2024**, *14*, 444. <https://doi.org/10.3390/app14010444>

Academic Editor: Nikolaos Koukouras

Received: 3 November 2023

Revised: 30 December 2023

Accepted: 2 January 2024

Published: 3 January 2024



Copyright: © 2024 by the authors. Licensee MDPI, Basel, Switzerland. This article is an open access article distributed under the terms and conditions of the Creative Commons Attribution (CC BY) license (<https://creativecommons.org/licenses/by/4.0/>).

1. Introduction

With the gradual depletion of near-surface resources, deep underground mining has become a strategic development direction. Currently, underground coal mining has reached below a thousand meters, and the frequency and intensity of disasters in deep and complex geological environments have risen significantly, posing challenges to the safe exploitation of underground resources [1]. Underground coal gasification (UCG) is a technology for controlled coal combustion located in underground reservoirs [2], which dramatically improves the utilization of coal resources. During the underground gasification of deep coal, the surrounding rock in the combustion cavity is exposed to a high-temperature environment, and this high-temperature effect may lead to damage and instability of the rock structure, which, in turn, affects the underground mining of coal [3]. In addition, in nuclear waste disposal projects [4], the excavation of tunnels, geothermal

energy recovery [5], and reinforcement and restoration projects after rock fire [6], the stability of the rock after high temperatures is crucial.

Currently, the physical and mechanical properties of rocks under the action of high temperature mainly focus on the elastic wave velocity, mass loss, elastic modulus, compressive strength, peak strain, porosity, and permeability [7–10]. Meng [11] found that the permeability, initial mercury injection, porosity, and fractal dimension of the pore structure of sandstone increased with the increase in temperature, which was relatively slow before 500 °C and increased rapidly after exceeding 500 °C. Alneasan [12] investigated the effect of temperature on the fracture characteristics of granite under three loading modes and found that the fracture behavior was temperature-dependent and could be changed from brittle to ductile. Wang [13] investigated the anisotropic mechanical behavior of oil shale from room temperature to 600 °C using a real-time high-temperature test system.

The acoustic emission (AE) technique is a method for detecting defects such as micro-cracks within rocks under stress and has been widely used for testing rock samples [14]. Rocks rapidly release elastic energy during crack expansion or deformation, generating transient pulses of elastic waves as AE events [15]. Du [16] obtained the influence laws on the strength properties and AE characteristics of rocks by analyzing the mineral composition and mineral grain size of rocks. Gao [17] investigated the acoustic emission activity of sandstone under perturbed stress paths and explored the relationship between acoustic emission parameters and fractal dimensions for the spatial and temporal distribution of acoustic emission activity during rock damage. Wang [18] conducted cyclic loading tests on granite, monitored the thermal damage evolution of the rock during the warming and cooling process in real time using a specially designed acoustic emission testing system, and established a thermal damage evolution model considering both the warming and cooling processes; the numerical results were in good agreement with the experimental results.

While grasping the changing pattern of such physicochemical properties, it is also necessary to explain this pattern through microscopic mechanisms. Currently, the commonly used means are scanning electron microscopy (SEM) [19], X-ray diffraction (XRD) [20], and computed tomography (CT) [21]. Tripathi [22] explored the effects of high temperatures on the microstructure, mineralogy, and physicochemical properties of the Barakar sandstone, which is one of the largest underground coal mine fire zones in the world, using scanning electron microscopy (SEM) and electron microprobe microanalysis. Based on the experimental results, the effects of temperature on the sandstone were categorized into three temperature zones. Using SEM and XRD, Sirdesai [23] found that the compound effect of the creation of new cracks and pores and the chemical change in the mineral composition under the action of high temperatures led to a reduction in the strength of the rock. The chemical change in mineral composition is an important factor affecting the physical and mechanical properties of rocks. For example, quartz transforms from α -quartz to β -quartz at 573 °C and then β -quartz to γ -quartz when the temperature reaches 870 °C [24]. Kaolinite will undergo a dehydroxylation reaction at 480–600 °C, changing into the meta kaolinite phase; at about 850–1000 °C, the meta kaolinite phase transforms into the Al-Si spinel phase [25].

In this paper, the effects of different temperatures (20–1200 °C) on the physical properties (color, mass, volume, density, and elastic wave velocity) and mechanical properties (uniaxial compressive strength, peak strain, and modulus of elasticity) of sandstones are mainly investigated by using an acoustic emission testing system to analyze the damage information during uniaxial compression, and SEM investigates the changes in the microstructure. On this basis, the effect produced by the heating rate on the mechanical properties of sandstone is further discussed. Compared with the existing studies, this paper collectively analyzes the intrinsic connection between the physical and mechanical properties, acoustic emission information, and macro and delicate damage patterns of sandstone after high temperature so that the study of the thermal damage mechanism of

sandstone is more systematic. The response characteristics of the macroscopic phenomenon and the microscopic mechanism are studied in more depth.

2. Materials and Methodology

2.1. Test Specimen

The sandstone used in this test was taken from the Tangjiahui mining area, Ordos City, Inner Mongolia Autonomous Region. The X-ray diffraction results show that its main mineral components are quartz, kaolinite, microcline, and muscovite, accounting for 58.1%, 28.7%, 7.9%, and 5.3%, respectively. In order to reduce the test dispersion, all the samples were taken from the same whole rock, with an average density that was 2.485 g/cm^3 at room temperature, and the elastic wave velocity was between 2.2 and 2.3 km/s. According to the recommended method of the International Society for Rock Mechanics (ISRM), the sandstone was prepared as a standard cylindrical specimen with a size of $\text{Ø}50 \text{ mm} \times 100 \text{ mm}$, and the sample was ground and polished to ensure the sample flatness ($<0.05 \text{ mm}$) and parallelism ($<0.02 \text{ mm}$). The test samples are shown in Figure 1.

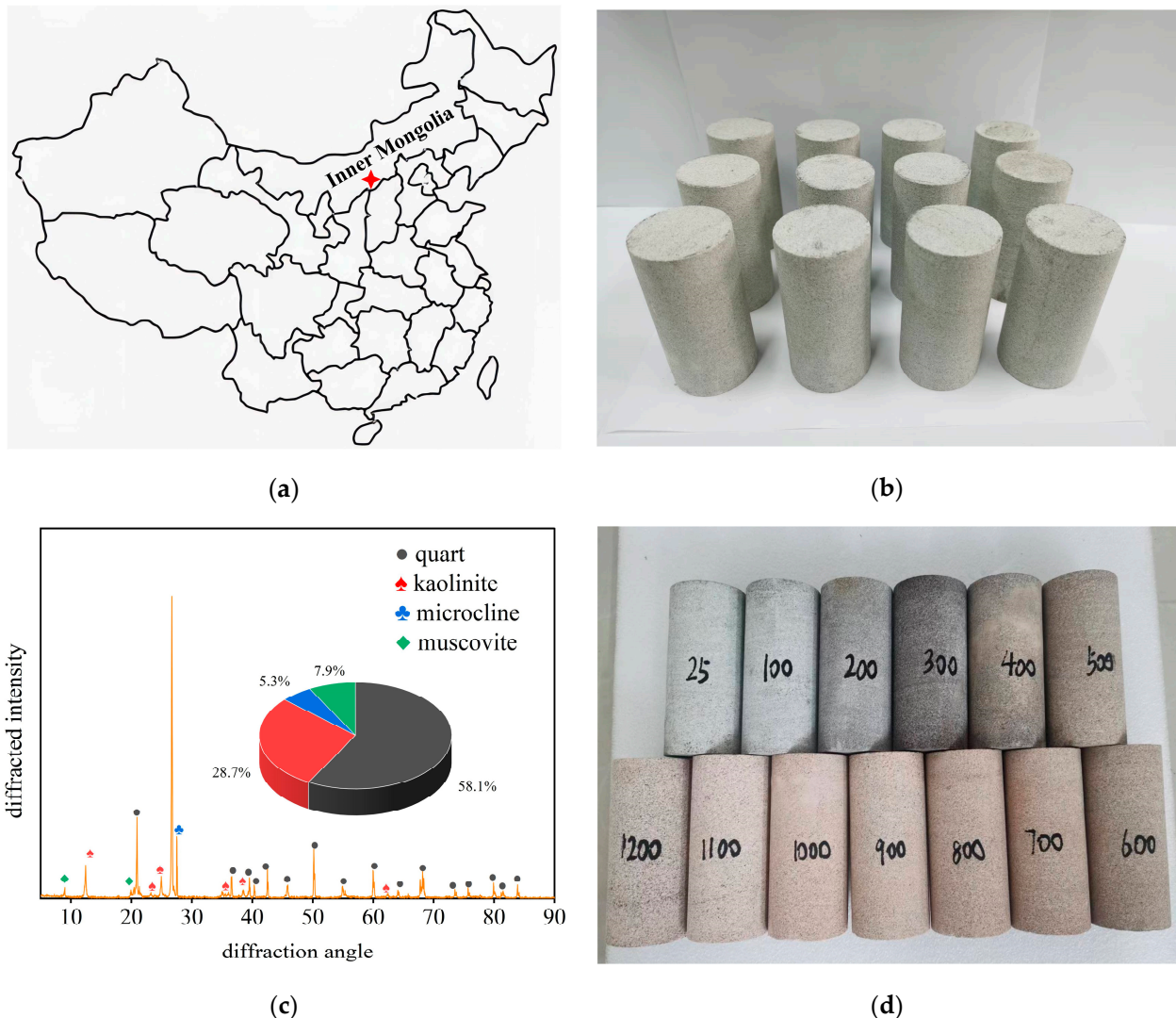


Figure 1. Test samples: (a) map of sampling locations; (b) specimen; (c) mineral composition of the specimen; (d) specimen after high temperature.

2.2. Test Equipment

The sandstone specimen was heated by a high-temperature chamber furnace with a chamber size of $200 \times 300 \times 200 \text{ mm}$, a maximum temperature of $1200 \text{ }^\circ\text{C}$, and a

temperature control accuracy of ± 1 °C. The elastic wave velocity of the specimen was determined using ultrasonic wave velocity tester. The uniaxial loading system adopts INSTRON 8802 fatigue tester. At the same time, the acoustic emission data of the specimen were collected with the DS5-8B acoustic emission monitoring system, a piezoelectric ceramic transducer, and adopted the double probe acquisition method to ensure complete data collection. The changes in micro-morphology after high temperature were analyzed by TESCAN-VEGA3 scanning electron microscope. The whole test system is shown in Figure 2.

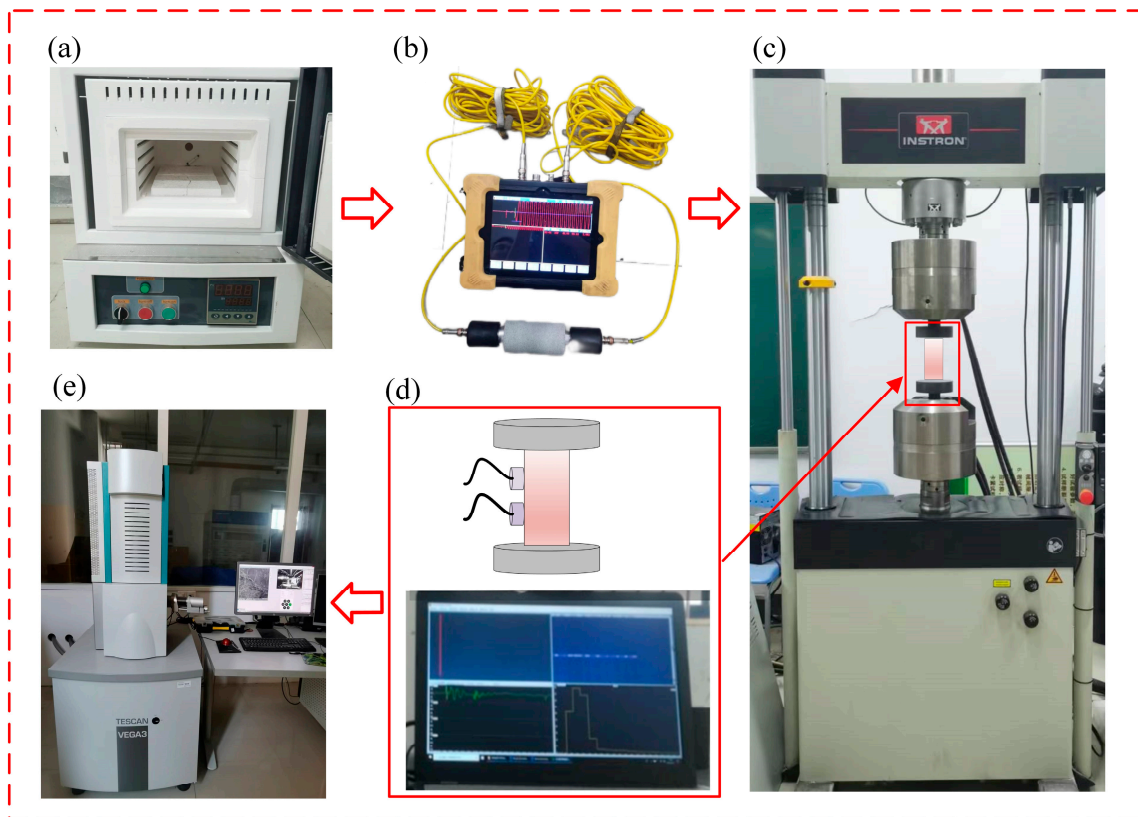


Figure 2. Testing equipment: (a) high-temperature box furnace; (b) wave velocity measuring instrument; (c) Instron testing machine; (d) AE monitoring system; (e) scanning electron microscope.

2.3. Test Method

After the sandstone specimens were prepared, the specimens' diameter, height, mass, and elastic wave velocity before and after heating were measured using vernier calipers, electronic scales, and wave velocity meters. The sandstone samples were heated in groups according to 100 °C, 200 °C,, 1200 °C, five samples in each group, the heating rate was 10 °C/min, and the samples were heated to the specified temperature for two hours and then cooled down naturally, and were numbered C1,, C12, and the samples at room temperature were numbered C0. In order to study the effect of heating rate on the mechanical properties of sandstone, the rock samples were heated up to 1200 °C according to four heating rates of 5 °C/min, 10 °C/min, 20 °C/min, and 30 °C/min, and each group of the same five samples was kept at a constant temperature for two hours and then naturally cooled down, which were numbered as V5, V10, V20, and V30, respectively. The heating process was the same for the two sets of samples numbered C12 and V10, so the same sample data will be used in the following discussion. The uniaxial compression test was conducted in a displacement-controlled manner with a loading rate of 0.5 mm/min, and the acoustic emission characteristics of the damage process were monitored at the same time of loading. The acoustic emission system was used in dual probe acquisition mode, and the preamplifier and threshold were set to 40 dB and 100 dB, respectively, to

reduce the ambient noise. Finally, the micro-damage characteristics were analyzed using a scanning electron microscope at room temperature–1200 °C and different heating rates.

3. Test Result

3.1. Physical Property Change

The physical properties of sandstone, such as color, mass, volume, density, and elastic wave velocity, change after experiencing high temperatures. Figure 1d shows the color change in sandstone after experiencing different temperatures. At room temperature, the sandstone is off-white, and at 100–200 °C, the color is similar to room temperature, and the change is not apparent. A significant darkening of the color was observed between 300 and 600 °C due to the combustion of organic matter. When the temperature increased to 700 °C, the color changed to reddish brown, presumably because the sandstone contains hematite reduced to iron at high temperatures. However, according to the XRD results in Figure 1c, no hematite material was found at room temperature, probably because the small content of diffraction peaks is not obvious.

The mass, volume, density, and elastic wave velocity of sandstone before and after high temperature were measured one by one, and four change rate indexes were defined: mass loss rate, volume expansion rate, density reduction rate, and elastic wave velocity reduction rate. These indexes are specifically defined as follows:

$$\eta_m = \frac{m_0 - m_1}{m_0}$$

$$\eta_v = \frac{v_1 - v_0}{v_1}$$

$$\eta_\rho = \frac{\rho_0 - \rho_1}{\rho_0}$$

$$\eta_p = \frac{p_0 - p_1}{p_0}$$

In the equations, η_m , η_v , η_ρ , η_p are the mass loss rate, volume expansion rate, density reduction rate, and wave speed reduction rate of sandstone before and after high temperature, respectively; m_0 , v_0 , ρ_0 , p_0 are the mass, volume, density, and elastic wave speed of sandstone before high temperature; m_1 , v_1 , ρ_1 , p_1 are the mass, volume, density, and elastic wave speed of sandstone after high temperature.

Figure 3 shows the variation in the physical properties of sandstone at different temperatures. Figure 3a reflects the variation in the mass loss rate with temperature, which increases with increasing temperature. Before 500 °C, the mass loss rate grows steadily, and the average value of the mass loss rate is between 0.68% and 1.65%. The mass loss rate increases rapidly at 500–600 °C, from 1.65% to 4.24%, an increase of 156.6%. After the heat treatment temperature of 600 °C, the mass loss rate lies between 4.24 and 4.99%, and the growth rate slows down. Figure 3b reflects the change in volume expansion rate with temperature, and the change in the volume expansion rate is not obvious before 500 °C. The volume of sandstone expanded rapidly from 500 to 600 °C, from 0.25% to 1.21%, and the volume expansion rate increased rapidly after 700 °C, and the volume expansion rate under heat treatment at 1200 °C reached 3.71%. Figure 3c shows the variation in the density reduction rate of sandstone with temperature, which is similar to the trend shown in Figure 3a. Figure 3d shows the variation in the wave velocity reduction rate with temperature, the wave velocity reduction rate increases from 4.34% to 13.18% before 500 °C, and the wave velocity reduction rate between 500 and 600 °C is 39.05% at 600 °C, which is 196.28% compared with that at 500 °C, and the wave velocity reduction rate increases to 62.21% at 1200 °C.

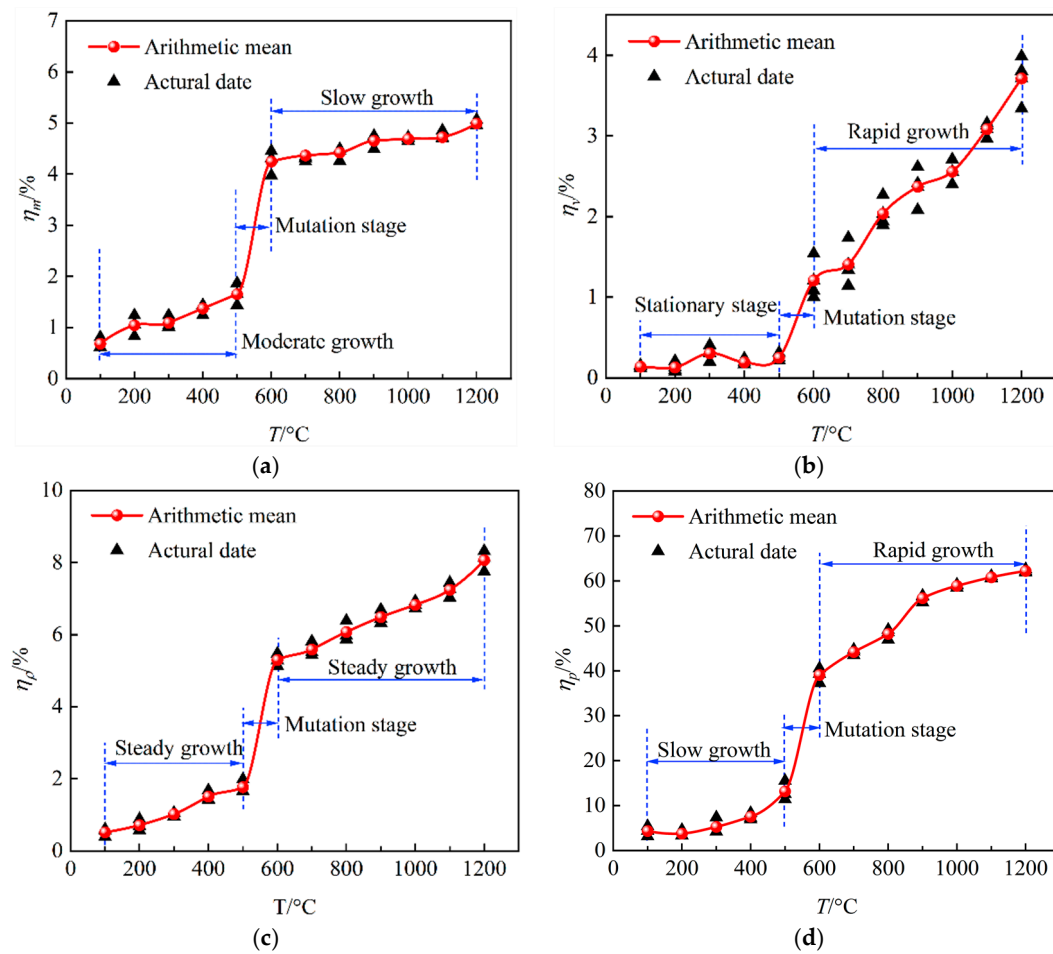


Figure 3. The variation in physical properties with temperature: (a) mass loss rate, (b) volume expansion rate, (c) density reduction rate, and (d) wave speed reduction rate.

It is summarized that the law of change in physical properties of sandstone with temperature is found to be mainly divided into three stages:

Stage I (100–500 °C): In this stage, the mass is steadily reduced due to the escape of water inside the sandstone [26]; the internal primary pores are contracted, the volume expansion is not apparent, and the density is reduced; the elastic wave velocity is slowly reduced.

Stage II (500–600 °C): This stage is the mutation stage. The main component of sandstone is quartz, which undergoes a phase change at 573 °C, from α -quartz to β -quartz, with rapid expansion in volume, and accompanied by the combustion of organic matter and decomposition of carbonate, which is the main reason for the sudden change in sandstone mass, volume, density, and longitudinal and transversal wave speeds at this stage.

Stage III (600–1200 °C): As the temperature rises, the decomposition of white muscovite and kaolinite becomes more severe, and the melting of the sandstone matrix and other reasons lead to a continued decrease in mass at this stage; an uneven expansion of the mineral particles, the formation and expansion of microcracks, and accelerated expansion of the volume; and a rapid decrease in the elastic wave velocity.

3.2. Uniaxial Compression Test

3.2.1. Uniaxial Compression Full Stress–Strain Curve

Figures 4 and 5 show the full stress–strain curves of the uniaxial compression tests at different temperatures and heating rates, respectively. In order to ensure the accuracy of the data to reduce the dispersion, the experimental curves with the largest and smallest

peak stresses have been removed, and the mechanical parameters of sandstone at different temperatures have been obtained by averaging the data of stress–strain curves, which are shown in Tables 1 and 2.

Table 1. Mechanical parameters at different temperatures.

$T/^\circ\text{C}$	σ/MPa	E/GPa	$\epsilon/10^{-2}$	$N_{\max}/10^3$	$\Sigma N/10^3$	σ_{IC}/MPa	σ_{ID}/MPa
25	55.91	5.29	1.47	2.48	13.25	39.72	50.57
100	57.24	5.53	1.43	2.32	14.66	42.05	56.36
200	59.83	5.78	1.36	3.07	15.71	44.06	58.60
300	65.88	6.23	1.49	3.65	20.53	51.62	63.71
400	79.36	6.66	1.76	4.52	27.72	57.38	76.97
500	94.76	6.90	1.87	6.27	38.68	70.67	91.41
600	89.03	6.05	2.31	5.99	40.67	58.69	80.96
700	87.12	5.77	2.42	5.23	43.19	52.33	75.71
800	85.59	5.51	2.55	4.83	48.25	51.58	75.36
900	81.91	5.32	2.66	3.78	47.14	43.31	73.24
1000	71.18	4.86	2.68	2.96	51.22	39.66	63.95
1100	58.15	3.54	2.69	2.01	52.31	31.26	45.36
1200	40.66	2.57	2.36	1.68	56.36	28.09	33.68

Table 2. Mechanical parameters at different heating rates.

$V\ (^{\circ}\text{C}/\text{min})$	σ/MPa	E/GPa	$\epsilon/10^{-2}$	$N_{\max}/10^3$	$\Sigma N/10^3$	σ_{IC}/MPa	σ_{ID}/MPa
5	51.14	3.13	2.69	1.85	55.82	30.96	45.02
10	40.66	2.57	2.36	1.68	54.51	28.09	37.55
20	38.46	2.52	2.35	1.54	51.66	26.84	37.21
30	32.54	2.16	2.32	1.39	49.97	25.66	36.68

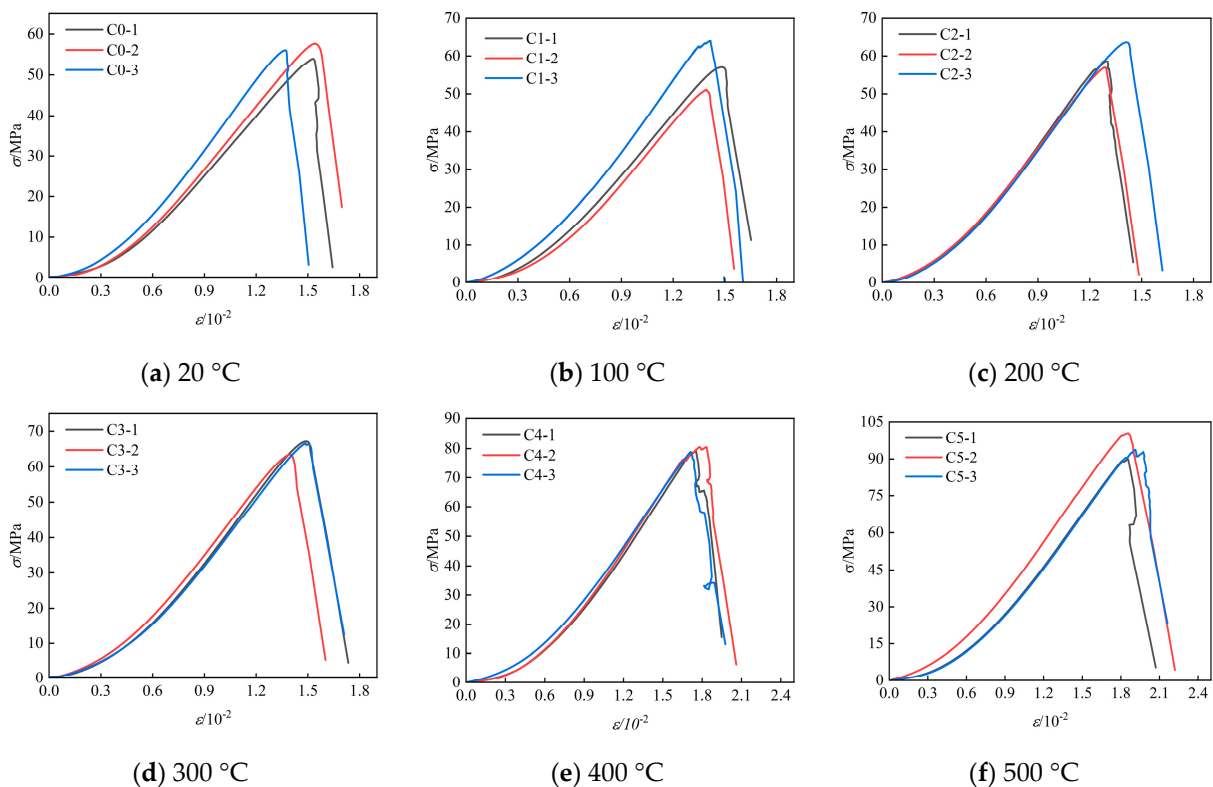


Figure 4. Cont.

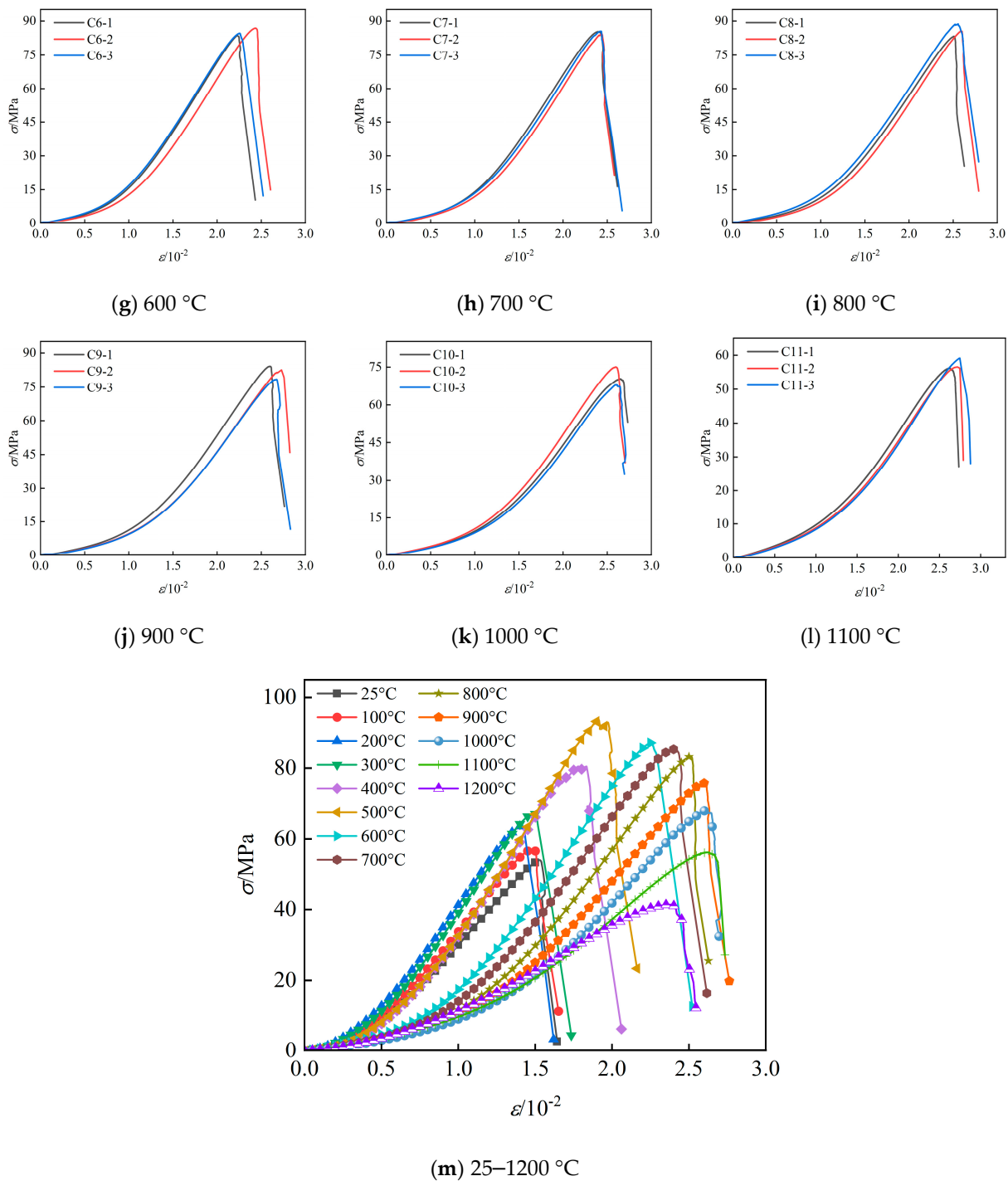


Figure 4. Total stress–strain curves at different temperatures.

From the figure, it can be seen that the stress–strain curve during uniaxial compression can be divided into four stages: compaction, elasticity, plastic deformation, and failure. First is the compaction stage, where the curve is up-concave, in which the microcracks inside the rock are gradually closed under the external load. The second is the approximate linear elasticity stage, where the stress–strain curve is approximated as an oblique straight line. At this stage, the external force is insufficient to produce new cracks or force the original cracks to undergo extension evolution, and the microscopic defects inside the rock do not change much, so the slope of this straight-line segment is taken as the average elastic modulus E of the rock. Subsequently, there is a plastic deformation stage, in which the stress–strain curve bends downward, the stress increase is slight, the axial strain increases rapidly, and

the microcracks begin to expand unsteadily. Finally, in the destruction stage, the sandstone specimen is rapidly destroyed and accompanied by a loud sound into the burst destruction. Different temperatures in the sandstone uniaxial compression process stress–strain curve characteristics are different; sandstone at 500 °C before the brittle damage is dominated, at 500 °C–600 °C sandstone began to be brittle to the ductile transition, compaction stage time increased significantly. At the same temperature of 1200 °C, the stress–strain curve shifted downward with the increase in heating rate.

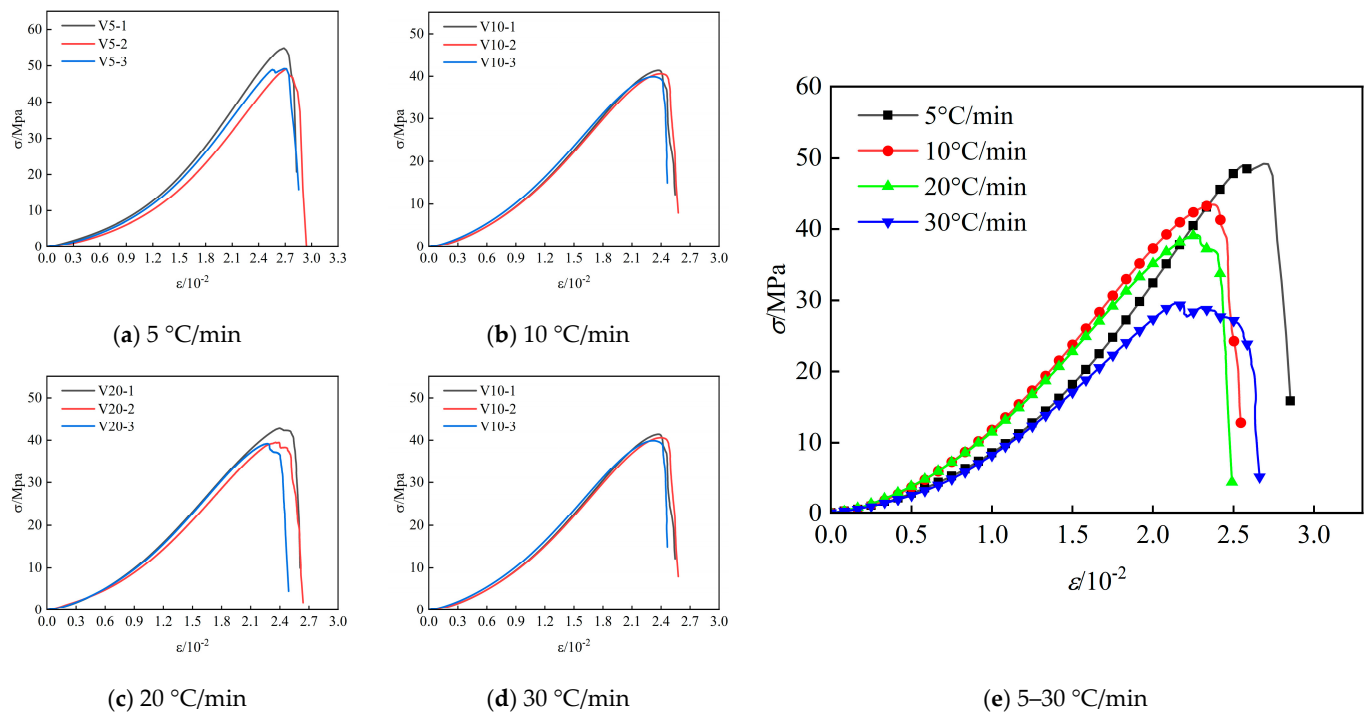


Figure 5. Total stress–strain curves at different heating rates at 1200 °C.

3.2.2. Variation Law of Peak Stress

According to the data in Tables 1 and 2, the variation patterns of peak stress σ , modulus of elasticity E , and peak strain ε of sandstone were investigated at different temperatures and heating rates. From Figure 6a, it can be seen that the peak stress of sandstone decreases with increasing temperature, and the peak stress reaches its maximum value at 500 °C. This trend is the same as that concluded by Hajpál [27] et al. but with different threshold temperatures. According to Zhang [28], by conducting uniaxial compression tests on sandstone at high temperatures, it was found that the compressive strength decreases with increasing temperature at temperatures from 25 to 200 °C and increases with increasing temperatures from 200 to 600 °C and then starts to decrease after 600 °C, and this variability is due to the difference in the mineral composition of the rock. According to the results of this paper, from room temperature to 500 °C, the peak stress of sandstone increases with temperature, from 55.91 MPa at room temperature (25 °C) to 94.76 MPa at 500 °C, an increase of 38.85 MPa or 69.48%. As the temperature continues to rise, the peak stress of sandstone decreases, and the peak stress at 1200 °C is 40.66 MPa, which is 54.1 MPa lower than that at 500 °C, a decrease of 57.09%. It is worth noting that temperatures between 100 °C and 1100 °C promote the compressive strength of sandstone relative to room temperature, and 1200 °C has a deteriorating effect on the compressive strength of sandstone.

Figure 6b shows the effect of heating rate on the peak stress of sandstone at 1200 °C. As the heating rate increases, the peak stress decreases, indicating that thermal shock decreases the compressive strength of sandstone. When the heating rate is 5 °C/min, the peak stress

is 51.14 MPa, and the peak stress is 32.54 MPa until the heating rate is 30 °C/min, which is a decrease of 17.6 MPa or 34.41%, and the average compressive strength of sandstone decreases by 0.704 MPa for every 1 °C/min increase in the heating rate.

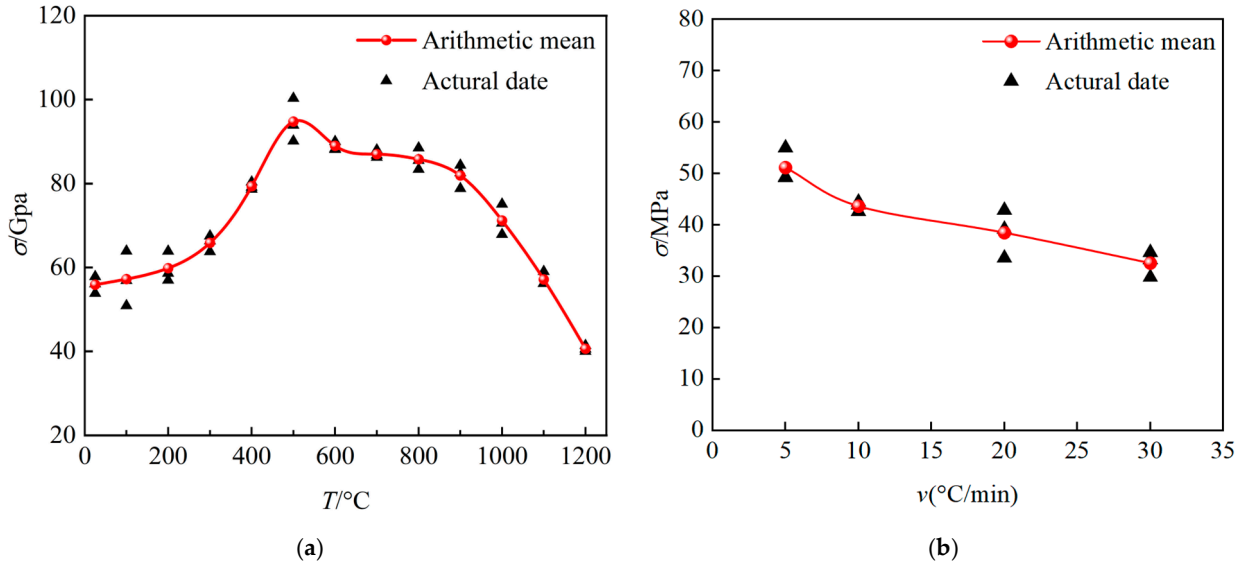


Figure 6. The peak stress varies with temperature and heating rate: (a) different temperatures; (b) different heating rates at 1200 °C.

3.2.3. Variation Law of Elastic Modulus

The average elastic modulus E of the sandstone was calculated by taking the approximate straight-line segment before the peak stress of the full stress–strain curve of the rock sample, and the variation rule of the average elastic modulus of the sandstone with temperature is given in Figure 7a. Before 500 °C, the elastic modulus increases approximately linearly with temperature, from 5.29 GPa at 25 °C to 6.90 GPa at 500 °C, an increase of 30.43%. Thereafter, the modulus of elasticity decreases with increasing temperature, with the fastest decrease from 1000 °C to 1200 °C. The modulus of elasticity at 1200 °C is 2.57 GPa, which is 62.7% lower than that at 500 °C.

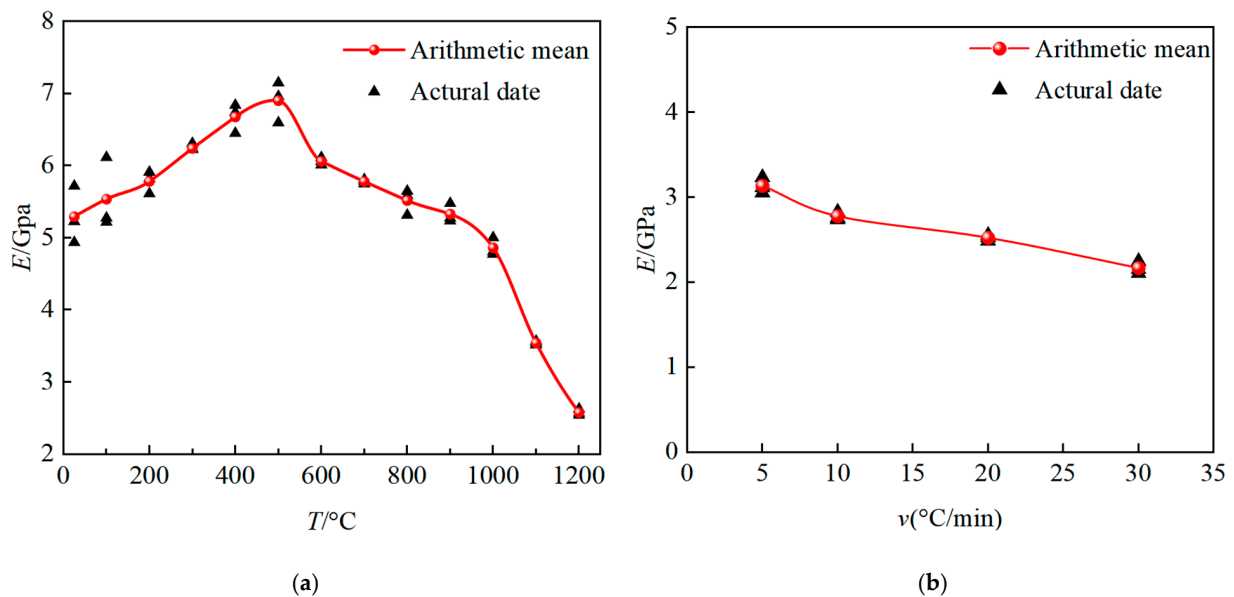


Figure 7. The elastic modulus varies with temperature and heating rate: (a) different temperatures; (b) different heating rates at 1200 °C.

Figure 7b shows the variation rule of elastic modulus E with the heating rate at 1200 °C: similar to the trend of peak stress, with the increase in heating rate, the elastic modulus is approximately linear decrease. The elastic modulus is 3.13 GPa at 5 °C/min and 2.16 GPa at 30 °C/min, which is 0.97 GPa lower than the previous year, a decrease of 31.29%.

3.2.4. Variation Law of Peak Strain

Figure 8a shows the variation rule of peak strain ε with temperature, which shows a general trend of decreasing and then increasing as the temperature increases, and the sandstone changes from brittle to ductile in the range of 500–600 °C. According to the results of Zhu [29], 800 °C is the initial temperature for the transition from brittle to ductile in the studied sandstones, and the different mineralogical composition of the studied sandstones also causes this difference. In this paper, it is found that the peak strain is 1.47×10^{-2} at room temperature 25 °C and 1.36×10^{-2} at 200 °C, which is a decrease of 7.48% compared with the same period, which is due to the closure of microfractures and the increase in the brittleness of sandstones due to the increase in temperature. Between 200 °C and 1100 °C, the peak strain increases continuously, and the peak strain at 1100 °C is 2.69×10^{-2} , a rise of 97.79%. When the temperature continues to increase to 1200 °C, the peak strain decreases again to 2.36×10^{-2} , which is due to the fact that the sandstone has been highly deteriorated at this temperature, and the ability to resist damage is greatly reduced.

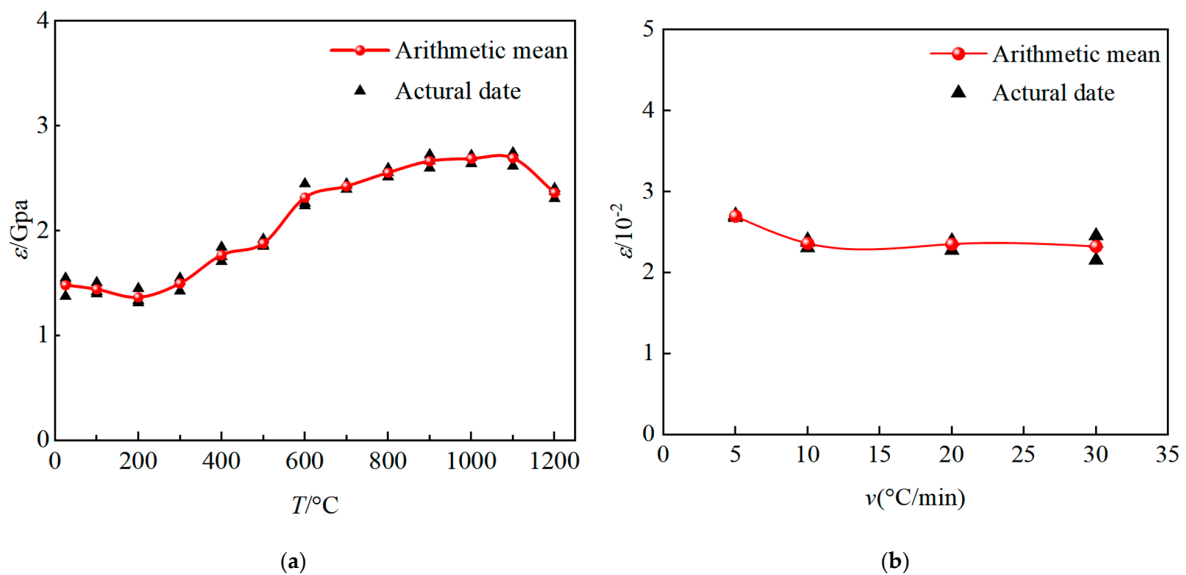


Figure 8. The peak strain varies with temperature and heating rate: (a) different temperatures; (b) different heating rates at 1200 °C.

Figure 8b shows the heating rate's effect on the sandstone's peak strain ε . The peak strain was 2.69×10^{-2} at the heating rate of 5 °C/min. The peak strains were 2.36×10^{-2} , 2.35×10^{-2} , and 2.32×10^{-2} at the heating rates of 10 °C/min, 20 °C/min, and 30 °C/min, respectively, with a fluctuation of not more than 2%, but compared to 5 °C/min, the peak strains were decreased by 12.26%, 12.63%, and 13.75%, respectively. This indicates that the rate of warming has little effect on the peak strain, and the temperature is the main influencing factor.

3.2.5. Macroscopic Failure Model

Rock is a non-homogeneous brittle material with internal discontinuities and inherent defects, and its fracture morphology is more complex and diverse after being affected by high temperatures. The destruction of this test sample is mainly divided into four kinds of destruction forms: single slope shear failure, X-shaped slope shear failure, splitting failure, and conical failure. According to Figure 9, the damage of sandstone at high temperatures

can be divided into four stages. In the first stage (25–300 °C), the damage of sandstone is mainly in the form of single slope shear failure and X-shaped slope shear failure. In this stage, the rock is more brittle, and the central part of the specimen does not have a large crack. Stage II (400–600 °C) and Stage III (700–900 °C) are more complex, with shear failure and splitting failure, increased bulkiness of the rock samples, small transverse microcracks around the rupture surface, and a rougher rupture surface. The difference is that Stage II is dominated by shear failure, while Stage III is dominated by splitting failure. In Stage IV (1000–1200 °C), the bearing capacity of sandstone is rapidly reduced, the damage state is severe, the specimen is a conical failure, and the fracture surface, due to friction, produces a large number of powdery particles.

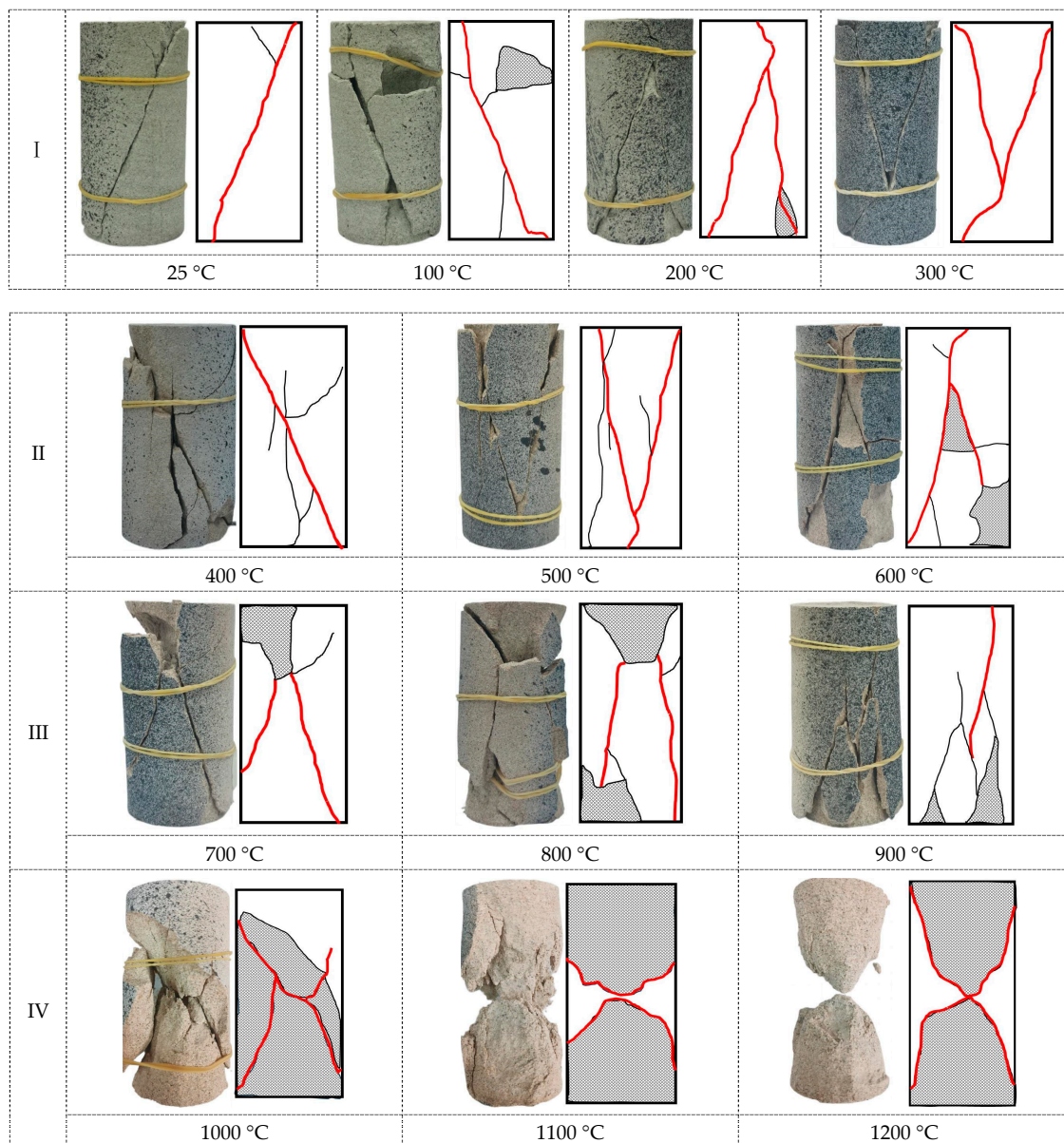


Figure 9. Macroscopic failure modes of sandstone at different temperatures.

4. Study on Acoustic Emission Characteristics

Rock in the load deformation and destruction process will produce acoustic emission information; this information can be expressed through the form of acoustic signals, when the acoustic signals generated by the internal damage of the rock break through the specific intensity and frequency thresholds, can be detected using the acoustic emission monitoring

instrument. Every time the acoustic signal is detected, a ringer count is performed, and the more ringer counts there are, the more acoustic signals are generated by the internal damage of the rock. In this paper, the ringer count N is used to analyze the acoustic emission characteristics of sandstone undergoing high temperature in the deformation and destruction process of uniaxial compression, and N_{max} and $\sum N$ denote the maximum value of the ringer counts and the cumulative ringer counts, respectively.

Figures 10 and 11 give the ringer counting characteristics during the sandstone’s uniaxial compressive deformation damage process after experiencing different high temperatures and warming rates, respectively; limited to space, only one typical rock sample characteristic is given for each temperature and warming rate.

From the figure, it can be seen that the variation in ringer counts is roughly divided into four stages. Stage I corresponds to the compression–density stage of the stress–strain curve. At this time, the rock samples in the lower stress under the role of some of the original microcracks within the closure of the acoustic emission events will be low. Stage II corresponds to the approximate elastic deformation stage, where the microdefects of the rock samples do not change much and are insufficient to form new microcracks. The rock mainly accumulates elastic energy at this stage, with fewer acoustic emission events, and the cumulative ring count curve grows linearly and slowly. Stages I and II can be considered a quiet period with few acoustic emission events. As the load continues to increase into Stage II, the low amplitude growth period, the internal microcracks of the rock samples are gradually generated and expanded, the acoustic emission events begin to tend to be active, the ringing counts increase significantly, and the slope of the cumulative ringing count curve begins to increase. In Stage IV, the internal newborn microcracks penetrate each other and start to change from stable to unstable expansion, the ringing counts increase rapidly, and the slope of the cumulative ringing count curve increases significantly. This stage is a period of high growth. The closer the rock releases more energy to the peak stress, the more pronounced the acoustic emission counts. Observing the change rule of ringing counts to predict the damage of sandstone can theoretically provide timely disaster warnings for underground engineering projects to a certain extent.

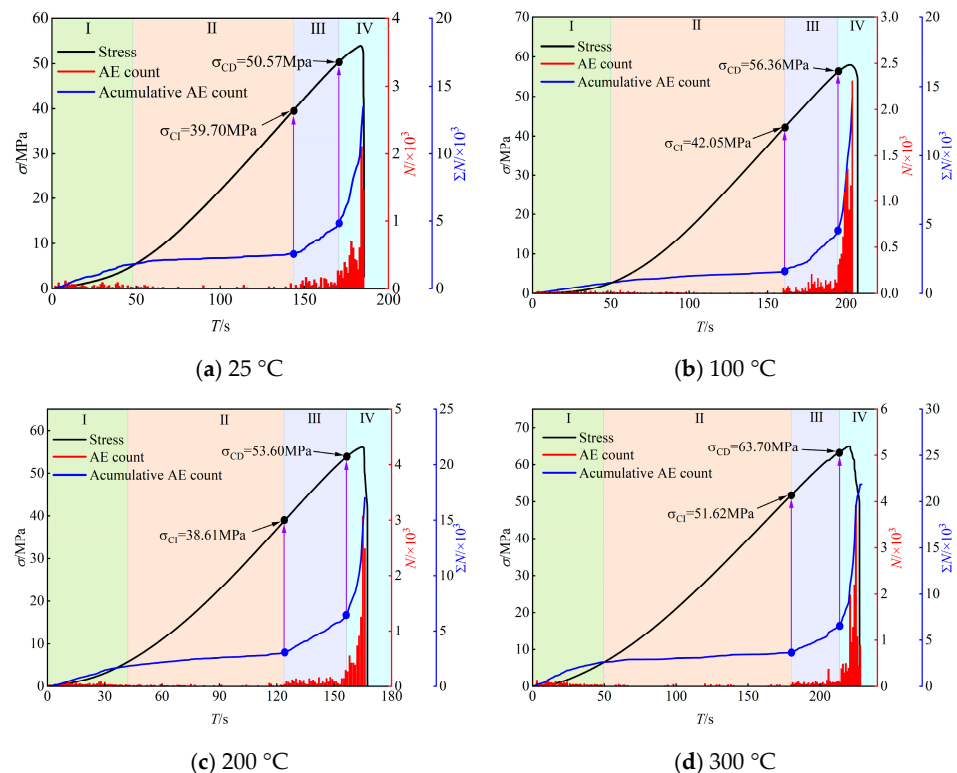


Figure 10. Cont.

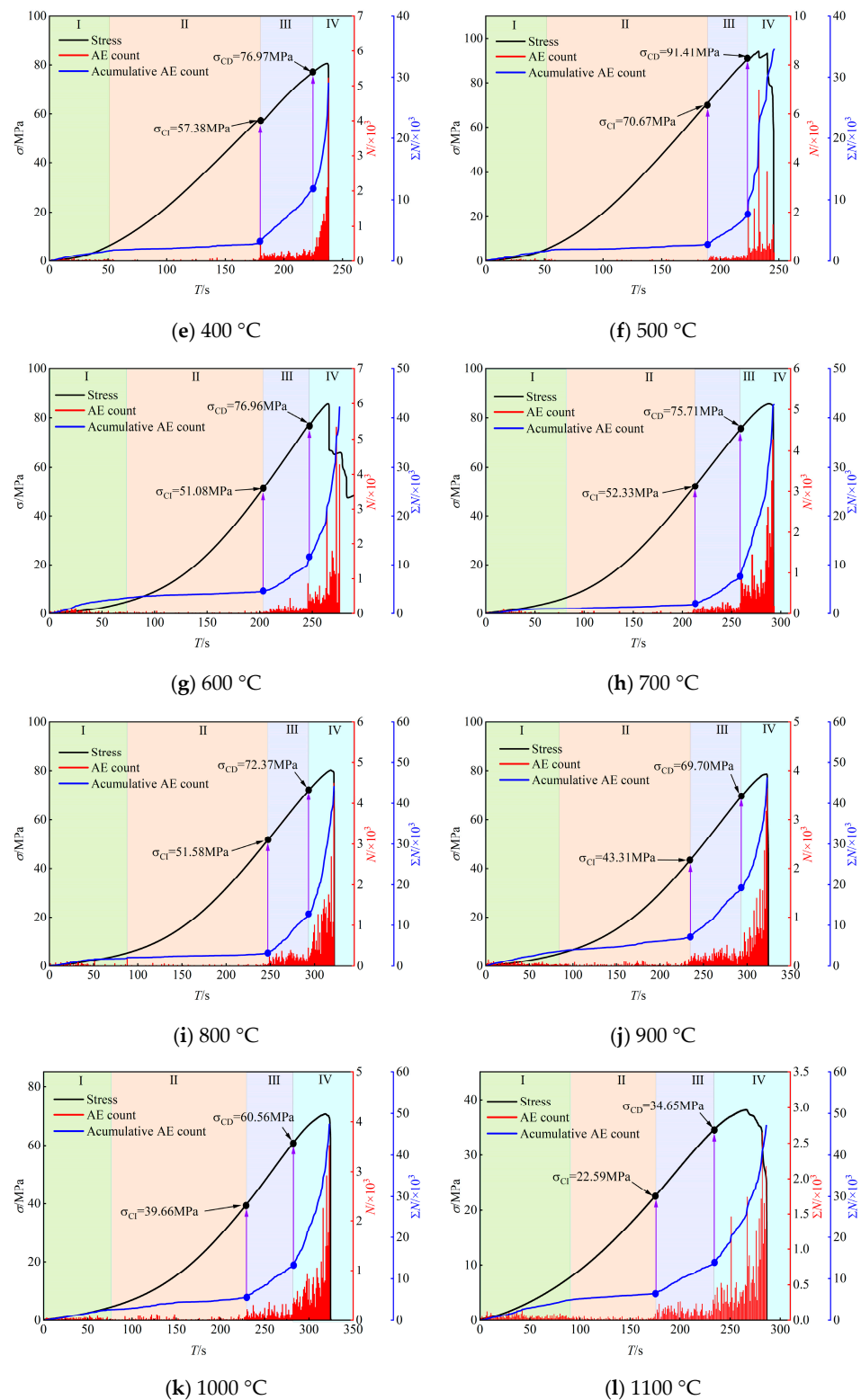


Figure 10. The variation law of acoustic emission characteristics at different temperatures.

4.1. Variation Law of Ringing Count

As shown in Figure 12, the maximum value of ringing count N_{max} increases and then decreases with increasing temperature, and the cumulative ringing count ΣN increases continuously with increasing temperature. The maximum and cumulative ringing counts at room temperature were 2.48×10^3 and 13.25×10^3 , respectively. With the continuous volatilization of water and the contraction of primary pores at elevated temperatures,

the brittleness and compressive strength of the sandstone were enhanced, the maximum ringing counts continued to increase and reached a peak at 500 °C, and the cumulative ringing counts also increased continuously in this temperature range. At 500 °C, the maximum ringing count and cumulative ringing count were 6.27×10^3 and 38.68×10^3 , respectively, an increase of 152.82% and 191.92% compared to room temperature. When the temperature is 600 °C, the acoustic emission signal of sandstone is more frequent due to the sandstone at this high temperature has formed damage; part of the work conducted with the external force is dissipated by the rock particles along the microdefective surface of the shear movement, the release of the elastic energy decreases, resulting in the acoustic emission ringing counts of the intensity of the reduction. The maximum ringing counts was 1.68×10^3 at the temperature increase to 1200 °C, which is 73% less than at 500 °C. As the ductility of sandstone is enhanced by high temperature, the thermal damage increases the microcracks inside the rock. Although the maximum intensity of the acoustic emission signal decreases, it occurs more frequently. The distribution area of the acoustic emission activity band is widened near the peak, increasing the cumulative ringing counts with the temperature. The maximum ringing count at 1200 °C is 56.36×10^3 , a 45.71% increase compared with 500 °C. The maximum ringing count at 1200 °C is 1.68×10^3 , which is a 73.21% decrease compared with that at 500.

Under the influence of a higher heating rate, the expansion of cracks and crystals in sandstone is more intense, and the rock damage is more serious. From Figure 13, the maximum ringing counts show a decreasing trend with the increase in heating rate, and the decrease in the overall ringing counts also leads to a decrease in the cumulative ringing counts with the increase in temperature because the heating rate does not have a significant effect on the activity range of acoustic emission at the same temperature. The maximum and cumulative ringing counts were 1.85×10^3 and 55.82×10^3 at a temperature increase rate of 5 °C/min. The maximum and cumulative ringing counts were 1.39×10^3 and 49.97×10^3 at a temperature increase rate of 30 °C/min, a decrease of 24.8% and 10.48%.

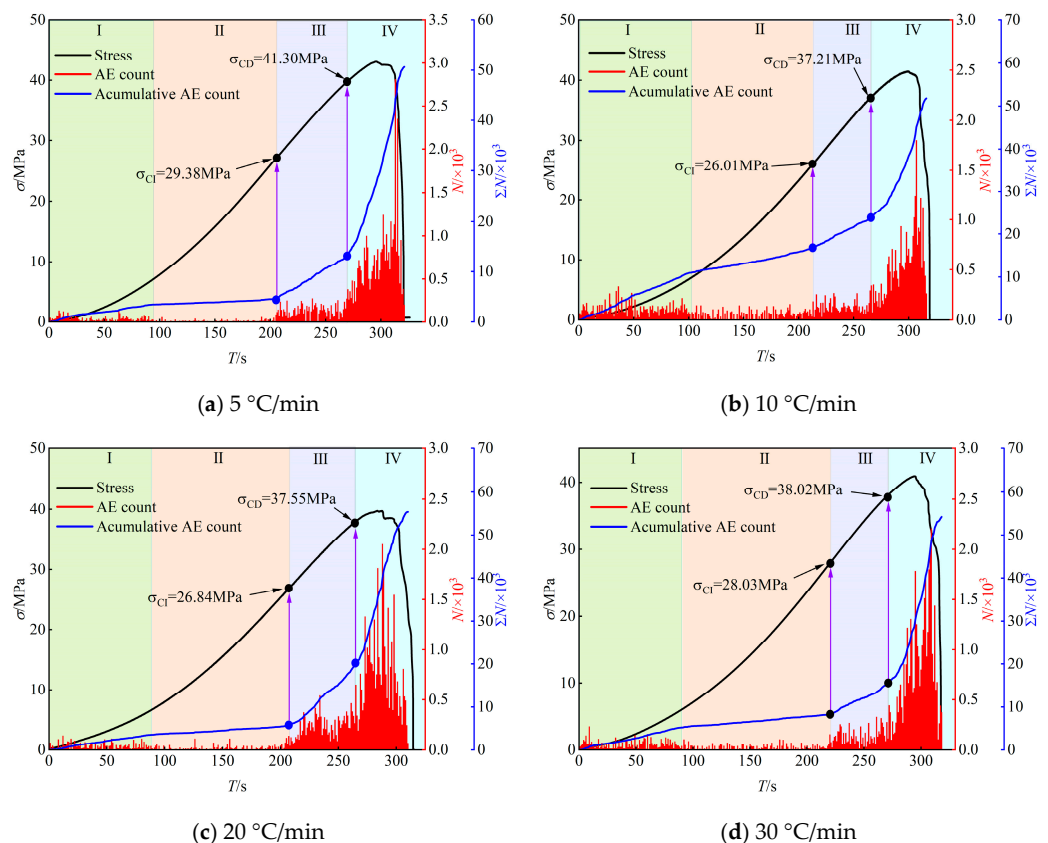


Figure 11. The variation law of acoustic emission characteristics at different heating rates at 1200 °C.

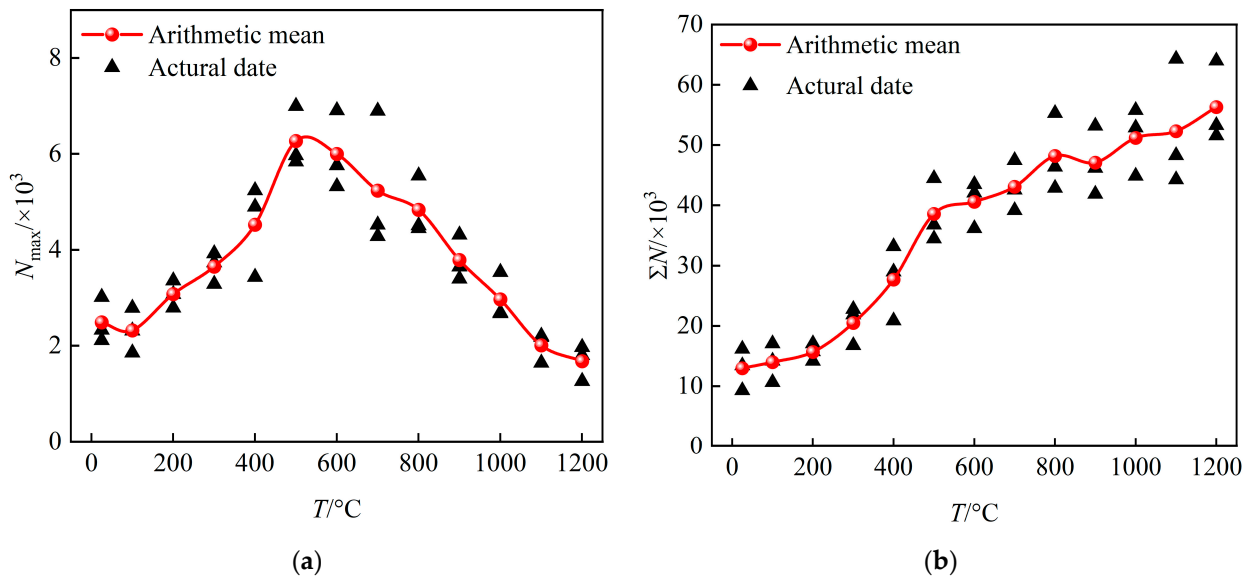


Figure 12. The change rule of the ringing counts at different temperatures: (a) maximum ringing count; (b) accumulative ringing count.

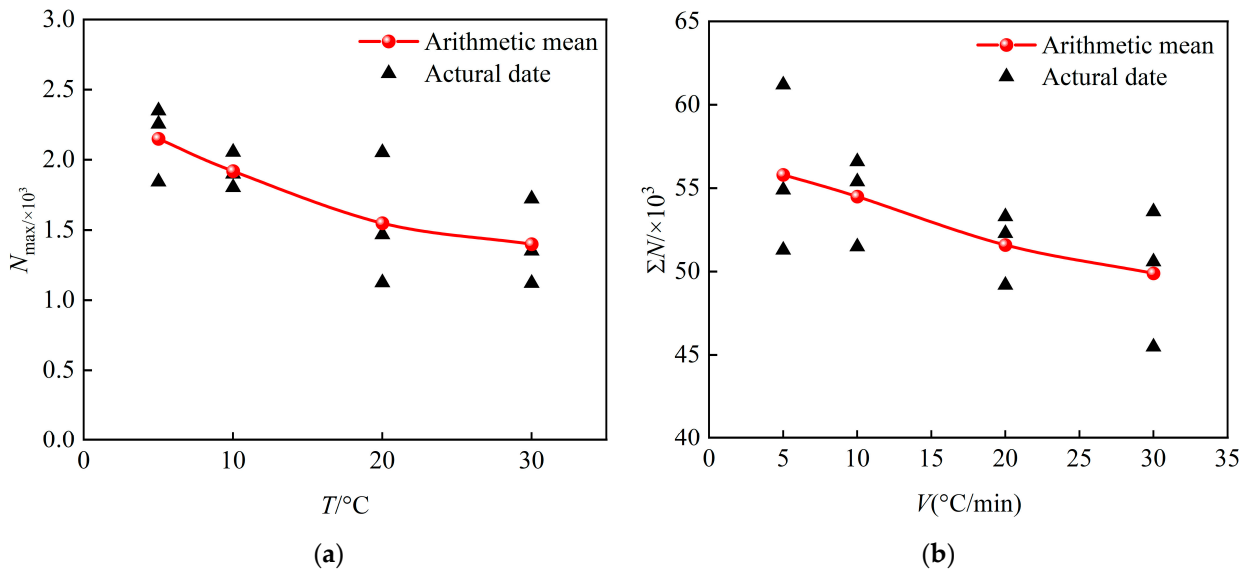


Figure 13. The change rule of the ringing counts at different heating rates: (a) maximum ringing count; (b) accumulative ringing count.

4.2. Variation Law of Stress Threshold

In the study of determining the crack initiation threshold stress σ_{CI} and damage threshold stress σ_{CD} using acoustic emission technology, scholars have given different methods. Wang [30] pointed out that the stress at the appearance of the first tensile crack in a rock sample is the crack initiation stress. It has been shown that the crack initiation stress and damage stress threshold can be effectively determined by using the mutation points of the acoustic emission cumulative ringer counting curve, in which the stress at the first mutation point can be taken as the crack initiation stress, and the stress at the sharp increase in the slope of the cumulative ringer counting curve can be taken as the crack damage stress threshold [31].

As can be seen from Figure 14a, with the increase in temperature, the crack initiation and damage threshold both show the trend of rising first and then decreasing, which is consistent with the characteristics of the change in peak stress with temperature. When

the temperature increases from room temperature to 500 °C, the crack initiation threshold increases from 39.72 MPa to 70.67 MPa, with an increase of 69.36%, and the damage threshold increases from 50.57 MPa to 91.41 MPa, with an increase of 80.75%, and the crack initiation and damage thresholds reach the maximum at 500 °C. After 600 °C, the crack initiation and damage thresholds began to decrease continuously; the crack initiation threshold at 1200 °C was 28.09 MPa, and the damage threshold was 33.68 MPa, which were 60.25% and 63.15% lower than that of 500 °C. The above analysis shows that the temperature has an essential effect on the crack initiation and damage thresholds and has a high correlation with the strength of sandstone.

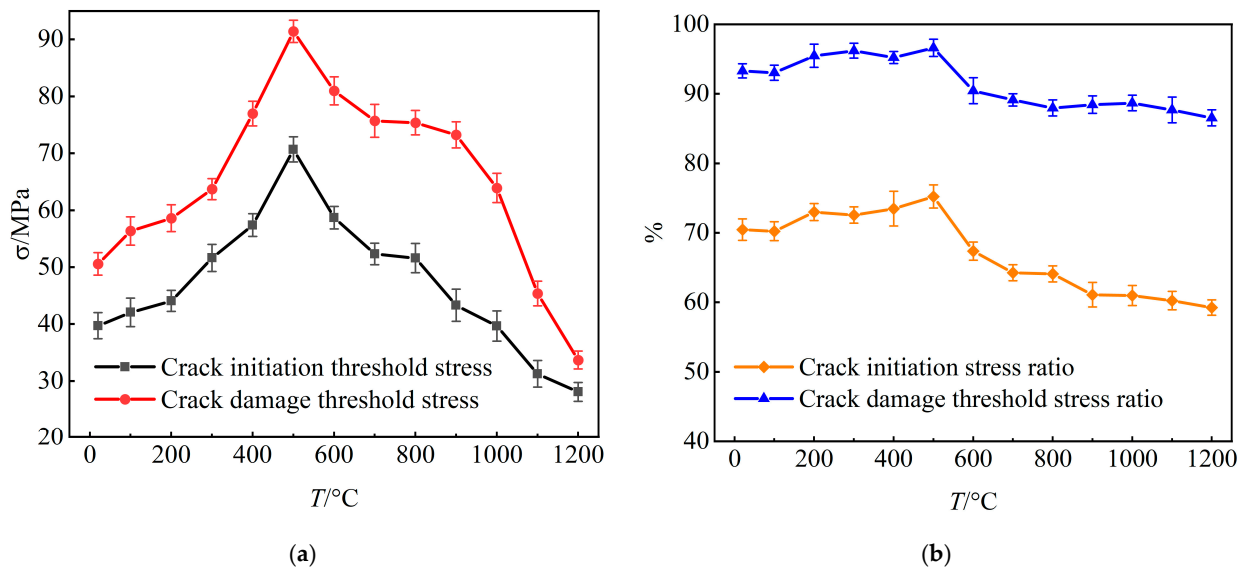


Figure 14. The variation law of stress threshold and proportion with temperature: (a) stress threshold; (b) proportion of stress threshold.

According to Figure 14b, the crack initiation threshold is about 58–76% of the peak stress, and the damage threshold is about 86–96% of the peak stress at room temperature up to 1200 °C, and the ratio shows a certain trend of change depending on the temperature. Before 500 °C, the percentage of crack initiation threshold and the percentage of damage threshold changed less but generally showed an increasing trend, the percentage of crack initiation threshold and the percentage of damage threshold increased from 70.46% and 93.31% to 75.23% and 96.61%, which indicated that the brittleness of the sandstone was enhanced to a certain extent in this temperature range, and the crack initiation threshold and damage threshold were closer to the peak stress. At 600 °C, the percentage of crack initiation threshold and damage threshold decreased to 67.38% and 90.44%, respectively, indicating that the physical and chemical properties of the rock in the temperature range of 500–600 °C have been greatly altered to produce certain damage. As the temperature continues to drop to 1200 °C, the percentage of crack initiation thresholds and damage thresholds show a decreasing trend, and the percentages of crack initiation thresholds and damage thresholds at 1200 °C are 59.26% and 89.54%, respectively, which indicates that the thermal damage will make the rock cracking damage at a lower stress level.

The heating rate also influences the crack initiation threshold and damage threshold and their percentage. From Figure 15a, the crack initiation threshold and damage threshold are 30.96 MPa and 45.52 MPa at 5 °C/min and 25.66 MPa and 36.68 MPa at 30 °C/min, which show a decreasing trend with the heating rate, and this trend is also very much correlated with the change in the peak stress by the heating rate. According to Figure 15b, the crack initiation threshold and damage threshold ratio are not significantly influenced by the heating rate and are more affected by the temperature.

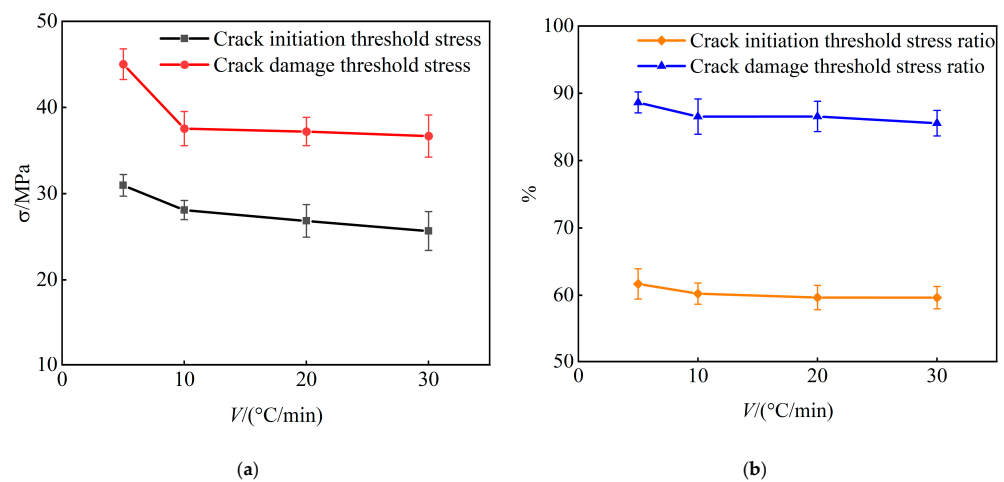


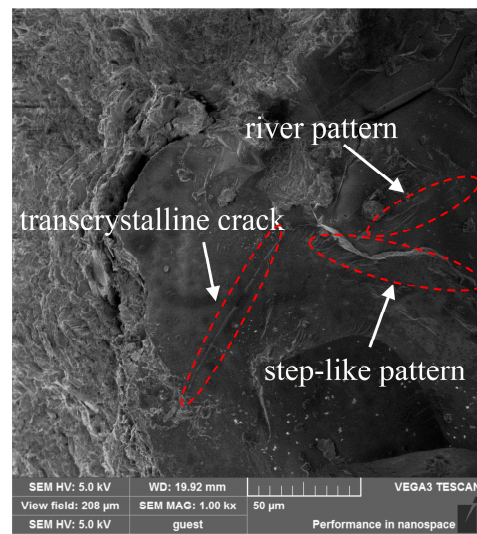
Figure 15. The variation law of stress threshold and proportion with heating rate at 1200 °C: (a) stress threshold; (b) proportion of stress threshold.

5. Discussion

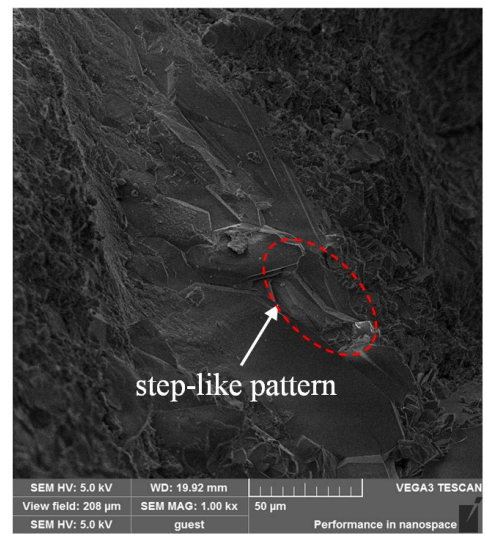
The previous section analyzed the mechanical properties and damage characteristics of sandstone at high temperatures with different heating rates using the uniaxial compression test and acoustic emission test. In this section, the temperature effect and heating rate of the micro-morphological characteristics of sandstone fracture surfaces were analyzed by using a scanning electron microscope to ultimately reveal the damage and rupture mechanism of sandstone under the action of high temperatures.

Figure 16 shows that pores and cavities already exist in the sandstone microstructure at room temperature. With the increase in temperature before 500 °C, the rock matrix and crystal particles are more tightly cemented, the thermal expansion of mineral particles leads to the closure of primary fissures, the degree of densification is increased, and the relative ratio of pores and cavities is significantly reduced compared with that at room temperature. At the same time, along with the evaporation of water, the brittleness of sandstone is enhanced, which also leads to the increase in peak stress and modulus of elasticity of sandstone with the increase in temperature, and the peak strain is not apparent with the change in temperature. From the fracture morphology, the fracture surface is mainly dominated by step-like patterns, river patterns, and trans crystalline cracks, which are typical brittle fracture patterns, and it can be concluded that the fracture surface of the sandstone at 500 °C shows significant brittle fracture.

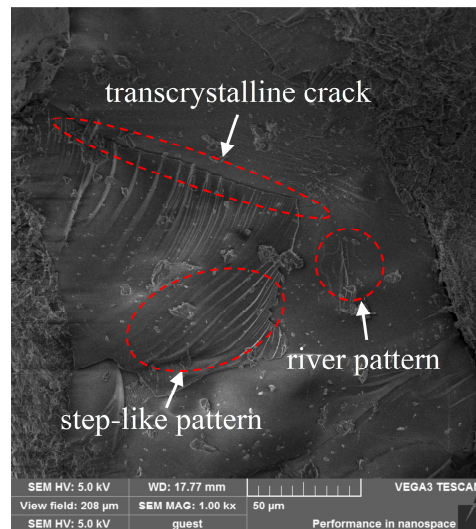
At 600 °C, thermal damage starts to occur in the sandstone structure, which is manifested by the sprouting of cracks and cavities in the crystal grains and matrix on the microscopic level and the gradual deterioration of the mechanical strength on the macroscopic level. At 1000 °C, the matrix of sandstone is no longer continuous and intact but is in a loose structure with a large number of microcracks, and there are a large number of thermal cracks on the crystal grains of sandstone, which results in the structure of the grain structure no longer being intact and generating a large number of fine particles and debris. The microcracks extend through each other, leading to a rapid decrease in the rock's load-bearing capacity, which also explains the increase in the decrease in peak stress and elastic modulus after 1000 °C in Figures 6a and 7a. Compared with the brittle fracture mode, more plastic deformation occurs on the fracture surface where ductile fracture occurs, and the fracture surface is not as flat and smooth as the brittle fracture, but a rougher fracture portion occurs. Comprehensive analysis of the fracture surface of sandstone after 600 °C ductile fracture morphology, mainly in the dimple, slip separation, and intergranular cracks, which is also a typical ductile fracture morphology, indicating that the fracture mode is a ductile fracture. From the fracture surface morphology, the brittle-ductile transition temperature of sandstone occurs between 500 and 600 °C, which is consistent with the previous conclusion.



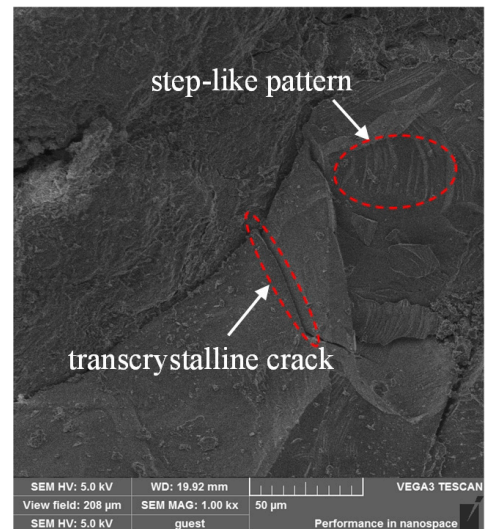
(a) 20 °C



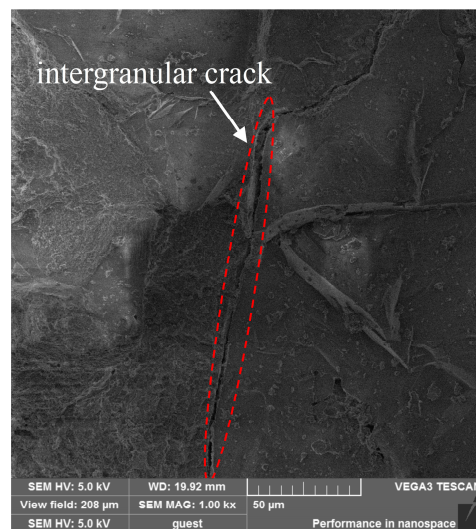
(b) 200 °C



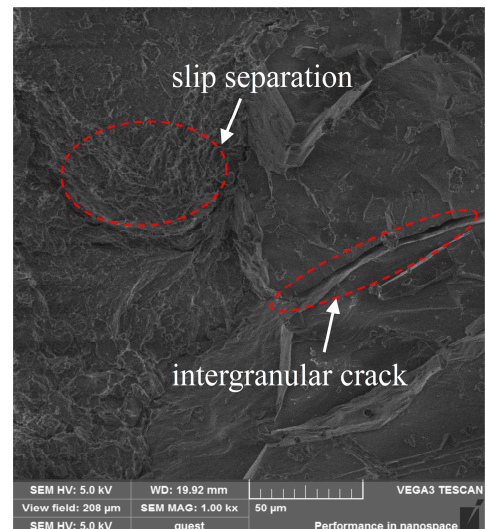
(c) 400 °C



(d) 500 °C



(e) 600 °C



(f) 800 °C

Figure 16. Cont.

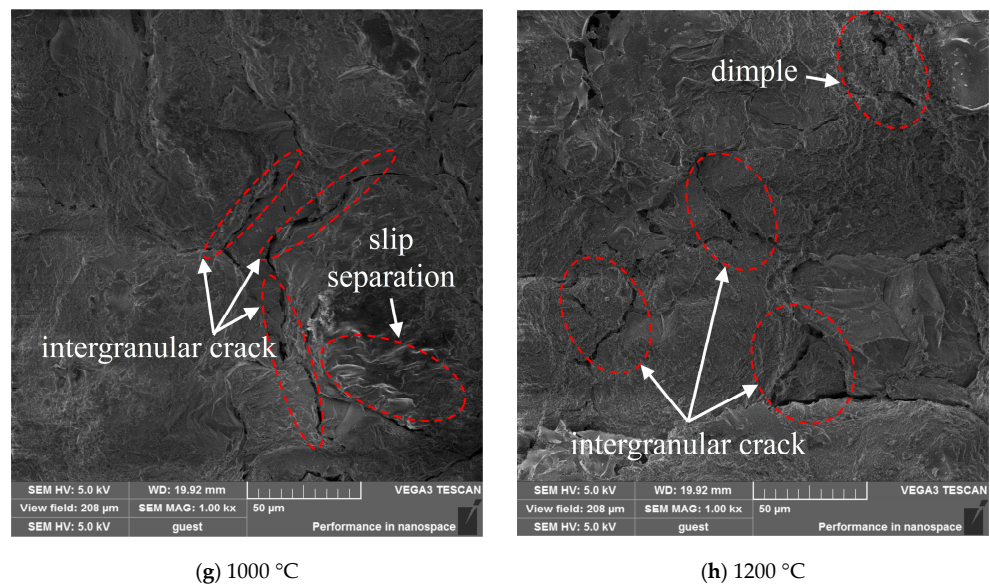


Figure 16. Micromorphology changes at different temperatures.

From Figure 17, a large number of cracks and pores already existed in the sandstone at 1200 °C, but with the increase in heating rate, the thermal damage and thermal rupture were more serious, which was manifested by the increase in surface roughness of the samples, and the obvious increase in crack width, length, and pore size, which led to the decrease in mechanical properties of the sandstone with the increase in heating rate. At 5 °C/min and 10 °C/min, the microscopic morphology is close to each other when the heating rate is relatively low, resulting in an increase in heating time; the mineral particles decomposed into smaller particles, resulting in a flatter cross-section. When the heating rate is 20 °C/min and 30 °C/min, the internal changes in the rock samples are drastic, and larger cracks and pores are produced under the strong thermal shock.

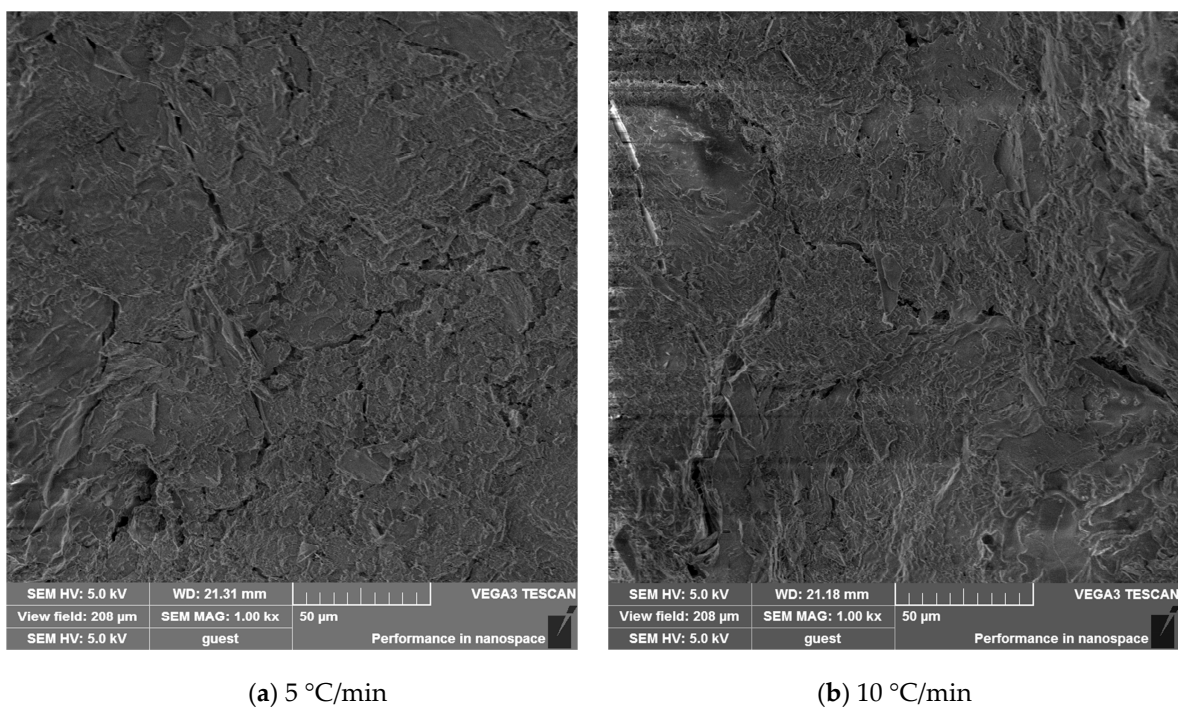


Figure 17. Cont.

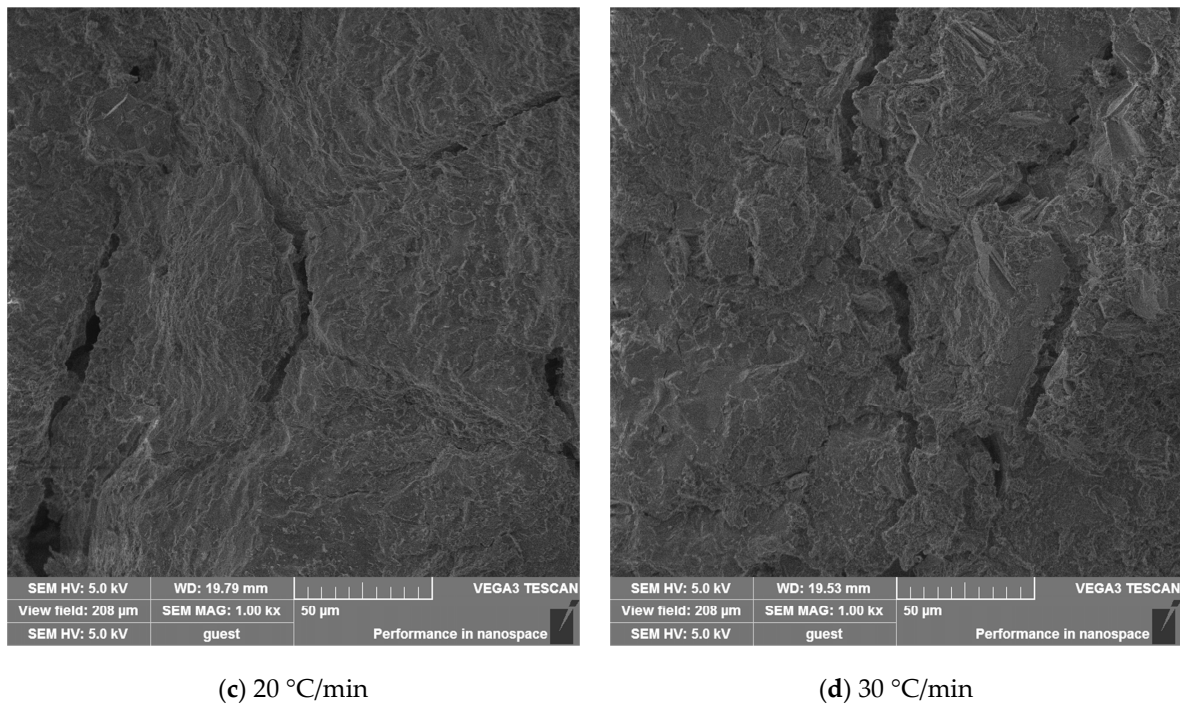


Figure 17. Micromorphology changes at different heating rates.

6. Conclusions

In order to study the macroscopic and microscopic properties of sandstone at high temperatures, uniaxial compression tests were carried out on sandstone at different temperatures as well as at different rates of warming to study the changes in the physical and mechanical properties of the sandstone and to analyze the mechanism of its damage evolution by acoustic emission technology and scanning electron microscopy, and the following conclusions were mainly drawn:

(1) As the temperature rises, sandstone physical properties appear in the phenomenon of mass reduction, volume expansion, density reduction, and wave velocity reduction, with the most apparent changes at 500–600 °C. The peak stress and modulus of elasticity of sandstone showed a tendency of increasing and then decreasing with temperature, with 500 °C as the threshold temperature, which was 69.48% and 30.43% higher than that of room temperature, and the peak strain showed a tendency of increasing with temperature, and slightly decreased at 200 °C and 1200 °C. The modulus of elasticity and peak stress show a decreasing trend with an increasing rate of warming, and the peak strain does not change much.

(2) The pattern of maximum ringing counts of sandstone is the same as that of its strength, and the maximum ringing counts increase and then decrease with the increase in temperature and increase with the increase in warming rate. The aggravation of thermal damage makes the ringing counts more frequent, and the cumulative ringing counts show an upward trend with the increase in both temperature and heating rate. The cracking threshold and damage threshold stresses and their ratios are highly correlated with the peak strength, and both of them show a specific decreasing trend with the increase in temperature, which indicates that the high-temperature treatment will cause the sandstone to crack prematurely.

(3) In the macro and microscopic damage pattern, before 500 °C, the thermal expansion within the sandstone internal crystals gradually closes the sandstone's pores and cracks, improving the sandstone's densification and mechanical properties. The macroscopic damage mode is dominated by shear damage, and the fracture morphology is mainly characterized by brittle morphology. After 600 °C, the large amount of development of cracks makes the structural integrity of sandstone deteriorate continuously, and the

mechanical properties gradually decrease. The macroscopic damage mode is dominated by cleavage damage, and the fracture surface is characterized by ductile morphology. By analyzing the changes in micromorphology under different heating rates at 1200 °C, the crack length and pore size will grow with the increase in the heating rate under thermal shock.

Author Contributions: Conceptualization, L.Z.; methodology, Y.Z.; validation, X.G. and P.W.; formal analysis, M.L.; data curation, F.Z.; writing—original draft preparation, L.Z. and Y.Z.; writing—review and editing, L.Z. and Y.Z.; visualization, P.W.; funding acquisition, L.Z. and M.L. All authors have read and agreed to the published version of the manuscript.

Funding: This research was funded by the National Natural Science Foundation of China (52074240, 52274140, and 51974296), the State Key Laboratory for GeoMechanics and Deep Underground Engineering, China University of Mining and Technology (SKLGDUEK2212), the Excellent Science and Technology Innovation Team of Jiangsu Province (Engineering Structural Safety under Complex Environmental), the sixth phase of Jiangsu Province “333 talents” training support special—card neck technology research.

Institutional Review Board Statement: Not applicable.

Informed Consent Statement: Not applicable.

Data Availability Statement: The data presented in this study are available on request from the corresponding author.

Acknowledgments: The authors are grateful for the equipment support provided by Xuzhou University of Technology.

Conflicts of Interest: The authors declare no conflict of interest.

References

1. Khadse, A.; Qayyumi, M.; Mahajani, S.; Aghalayam, P. Underground coal gasification: A new clean coal utilization technique for India. *Energy* **2007**, *32*, 2061–2071. [\[CrossRef\]](#)
2. Xin, L.; Chao, L.; Liu, W.; Xu, M.; Xie, J.; Han, L.; An, M. Change of sandstone microstructure and mineral transformation nearby UCG channel. *Fuel Process. Technol.* **2021**, *211*, 106575. [\[CrossRef\]](#)
3. Róg, L. Vitrinite reflectance as a measure of the range of influence of the temperature of a georeactor on rock mass during underground coal gasification. *Fuel* **2018**, *224*, 94–100. [\[CrossRef\]](#)
4. Chen, Y.; Hu, S.; Wei, K.; Hu, R.; Zhou, C.; Jing, L. Experimental characterization and micromechanical modeling of damage-induced permeability variation in Beishan granite. *Int. J. Rock Mech. Min. Sci.* **2014**, *71*, 64–76. [\[CrossRef\]](#)
5. Horseman, S.T.; McEwen, T.J. Thermal constraints on disposal of heat-emitting waste in argillaceous rocks. *Eng. Geol.* **1996**, *41*, 5–16. [\[CrossRef\]](#)
6. Bi, J.; Liu, P.; Gan, F. Effects of the cooling treatment on the dynamic behavior of ordinary concrete exposed to high temperatures. *Constr. Build. Mater.* **2020**, *248*, 118688. [\[CrossRef\]](#)
7. Li, M.; Wang, D.; Shao, Z. Experimental study on changes of pore structure and mechanical properties of sandstone after high-temperature treatment using nuclear magnetic resonance. *Eng. Geol.* **2020**, *275*, 105739. [\[CrossRef\]](#)
8. Yang, S.-Q.; Huang, Y.-H.; Tian, W.-L.; Yin, P.-F.; Jing, H.-W. Effect of High Temperature on Deformation Failure Behavior of Granite Specimen Containing a Single Fissure Under Uniaxial Compression. *Rock Mech. Rock Eng.* **2019**, *52*, 2087–2107. [\[CrossRef\]](#)
9. Shen, Y.-J.; Zhang, Y.-L.; Gao, F.; Yang, G.-S.; Lai, X.-P. Influence of Temperature on the Microstructure Deterioration of Sandstone. *Energies* **2018**, *11*, 1753. [\[CrossRef\]](#)
10. Yavuz, H.; Demirdag, S.; Caran, S. Thermal effect on the physical properties of carbonate rocks. *Int. J. Rock Mech. Min. Sci.* **2010**, *47*, 94–103. [\[CrossRef\]](#)
11. Meng, T.; Yongbing, X.; Ma, J.; Yue, Y.; Liu, W.; Zhang, J.; Erbing, L. Evolution of permeability and microscopic pore structure of sandstone and its weakening mechanism under coupled thermo-hydro-mechanical environment subjected to real-time high temperature. *Eng. Geol.* **2021**, *280*, 105955. [\[CrossRef\]](#)
12. Alneasan, M.; Alzo’ubi, A.K. Temperature Effect on the Fracture Behavior of Granite Under Three Loading Modes (I, I/II, and II). *Rock Mech. Rock Eng.* **2023**, *56*, 2197–2211. [\[CrossRef\]](#)
13. Wang, G.; Yang, D.; Liu, S.; Fu, M.; Wang, L. Experimental Study on the Anisotropic Mechanical Properties of Oil Shales Under Real-Time High-Temperature Conditions. *Rock Mech. Rock Eng.* **2021**, *54*, 6565–6583. [\[CrossRef\]](#)
14. Lockner, D. The role of acoustic emission in the study of rock fracture. *Int. J. Rock Mech. Min.* **1993**, *30*, 883–899. [\[CrossRef\]](#)
15. Geng, J.; Sun, Q.; Zhang, Y.; Cao, L.; Zhang, W. Studying the dynamic damage failure of concrete based on acoustic emission. *Constr. Build. Mater.* **2017**, *149*, 9–16. [\[CrossRef\]](#)

16. Du, K.; Sun, Y.; Zhou, J.; Khandelwal, M.; Gong, F. Mineral Composition and Grain Size Effects on the Fracture and Acoustic Emission (AE) Characteristics of Rocks Under Compressive and Tensile Stress. *Rock Mech. Rock Eng.* **2022**, *55*, 6445–6474. [[CrossRef](#)]
17. Gao, Y.; Lan, D.; Yang, S.; Hou, P.; Wang, Y.; Ding, F. The Acoustic Emission Behavior and Its Fractal Characteristics of the Sandstone Under the Disturbance Stress Paths. *Rock Mech. Rock Eng.* **2023**, *56*, 5487–5511. [[CrossRef](#)]
18. Wang, Z.; Zhou, G.; Ge, X. Experimental study on damage characteristics of Beishan granite under single loading and multiple loading with AE techniques. *Sci. Rep.* **2023**, *13*, 8767. [[CrossRef](#)]
19. Zuo, J.; Xie, H.; Zhou, H. Investigation of meso-failure behavior of rock under thermal-mechanical coupled effects based on high temperature SEM. *Sci. China Phys. Mech. Astron.* **2012**, *55*, 1855–1862. [[CrossRef](#)]
20. Perez-Rodriguez, J.L.; Duran, A.; Perez-Maqueda, L.A. Thermal study of unaltered and altered dolomitic rock samples from ancient monuments: The case of Villarcayo de Merindad de Castilla la Vieja (Burgos, Spain). *J. Therm. Anal. Calorim.* **2011**, *104*, 467–474. [[CrossRef](#)]
21. Mahanta, B.; Vishal, V.; Ranjith, P.G.; Singh, T.N. An insight into pore-network models of high-temperature heat-treated sandstones using computed tomography. *J. Nat. Gas Sci. Eng.* **2020**, *77*, 103227. [[CrossRef](#)]
22. Tripathi, A.; Gupta, N.; Singh, A.K.; Mohanty, S.P.; Rai, N.; Pain, A. Effects of Elevated Temperatures on the Microstructural, Physico-Mechanical and Elastic Properties of Barakar Sandstone: A Study from One of the World's Largest Underground Coalmine Fire Region, Jharia, India. *Rock Mech. Rock Eng.* **2021**, *54*, 1293–1314. [[CrossRef](#)]
23. Sirdesai, N.N.; Singh, T.N.; Pathegama Gamage, R. Thermal alterations in the poro-mechanical characteristic of an Indian sandstone—A comparative study. *Eng. Geol.* **2017**, *226*, 208–220. [[CrossRef](#)]
24. Hajpal, M.; Torok, A. Mineralogical and colour changes of quartz sandstones by heat. *Environ. Geol.* **2004**, *46*, 311–322. [[CrossRef](#)]
25. Zhang, W.; Sun, Q.; Zhu, Y.; Guo, W. Experimental study on response characteristics of micro–macroscopic performance of red sandstone after high-temperature treatment. *J. Therm. Anal. Calorim.* **2018**, *136*, 1935–1945. [[CrossRef](#)]
26. Sun, Q.; Lu, C.; Cao, L.; Li, W.; Geng, J.; Zhang, W. Thermal properties of sandstone after treatment at high temperature. *Int. J. Rock Mech. Min. Sci.* **2016**, *85*, 60–66. [[CrossRef](#)]
27. Ranjith, P.G.; Viete, D.R.; Chen, B.J.; Perera, M.S.A. Transformation plasticity and the effect of temperature on the mechanical behaviour of Hawkesbury sandstone at atmospheric pressure. *Eng. Geol.* **2012**, *151*, 120–127.
28. Zhang, L.; Mao, X.; Lu, A. Experimental study on the mechanical properties of rocks at high temperature. *Sci. China Ser. E Technol. Sci.* **2009**, *52*, 641–646. [[CrossRef](#)]
29. Zhu, J.; Qi, T.; Li, J.; Cheng, Z.; Zhang, Y. The Effects of High Temperature on Crack Propagation and Failure Characteristics of Sandstone. *Rock Mech. Rock Eng.* **2023**, *56*, 5753–5779. [[CrossRef](#)]
30. Wang, X.; Wen, Z.; Jiang, Y.; Huang, H. Experimental Study on Mechanical and Acoustic Emission Characteristics of Rock-Like Material Under Non-uniformly Distributed Loads. *Rock. Mech. Rock. Eng.* **2018**, *51*, 729–745. [[CrossRef](#)]
31. Eberhardt, E.; Stead, D.; Stimpson, B. Quantifying progressive pre-peak brittle fracture damage in rock during uniaxial compression. *Int. J. Rock Mech. Min. Sci.* **1999**, *36*, 361–380. [[CrossRef](#)]

Disclaimer/Publisher's Note: The statements, opinions and data contained in all publications are solely those of the individual author(s) and contributor(s) and not of MDPI and/or the editor(s). MDPI and/or the editor(s) disclaim responsibility for any injury to people or property resulting from any ideas, methods, instructions or products referred to in the content.